ASSEMBLY OF A NOVEL CAVITAND UTILIZING DYNAMIC COVALENT BOND FORMATION

by

JAMES LYLE BENNETT

A thesis submitted to the

Graduate School-New Brunswick

Rutgers, the State University of New Jersey

In partial fulfillment of the requirements

For the degree of

Master of Science

Graduate Program in Chemistry

Written under the direction of

Ralf Warmuth, Ph.D.

And approved by

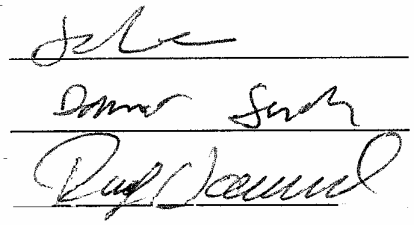

New Brunswick, New Jersey

October, 2008

ABSTRACT OF THE THESIS

Assembly of a Novel Cavitand Utilizing Dynamic Covalent Bond Formation

By James Lyle Bennett

Thesis Director:

Ralf Warmuth, Ph.D.

Molecular assembly which utilizes dynamic covalent bonding is reported. Previously unreported cavitand **19** was synthesized and is shown to assemble into structure **20** which is composed of four cavitands and eight ethylenediamine by the formation of sixteen imine bonds.

DEDICATION

I dedicate this work to Oliver O. Bennett, Sr. for his desire that all his grandchildren achieve their educational goals.

TABLE OF CONTENTS

LIST OF FIGURES

LIST OF ABBREVEIATIONS

THAP	2',4',6'-trihydroxyacetophenone
THF	tetrahydrofuran
DMF	N,N-dimethylformamide
DMA	N,N-dimethylacetamide
EtOAc	ethyl acetate
TFA	triflouroacetic acid
TEA	triethylamine
DMSO	dimethylsulfoxide
MEK	methyl ethyl ketone
DVB	Divinylbenzene
NMR	Nuclear Magnetic Resonance
DCC	Dynamic Covalent Chemistry
t-BuLi	tert-butyl lithium
n-BuLi	normal-butyl lithium
MeOH	Methanol
HPLC	High Pressure Liquid Chromatography
MALDI-TOF	Matrix Assisted Laser Desorption Ionization – Time Of Flight
MS	Mass Spectroscopy
GPC	Gel Permeation Chromatography
aq	aqueous
i-Pr	iso-propyl
ArLi	aryl lithium

CHAPTER 1

Introduction

Host-guest chemistry pioneer Donald Cram explored molecular encapsulation utilizing the unique characteristics of the cavitand: namely, a cavitand is a rigid cup shaped molecule.[1] Dimerization of two cavitands was reported by Cram and yields a molecular container which contains an internal cavity that permanently incarcerated one guest molecule, such as Cs^{+1}, or a solvent molecule present during the reaction (Figure 1).[2] Cram coined the term 'carcerand' for guestless cavitand dimers and 'carceplex' for the complex of the carcerand and permanently entrapped guest molecule. A 'hemicarceplex' is a carcerand/guest complex in which the guest may enter or escape the carcerand's cavity at high temperatures, but is stable at ambient temperatures.[3]

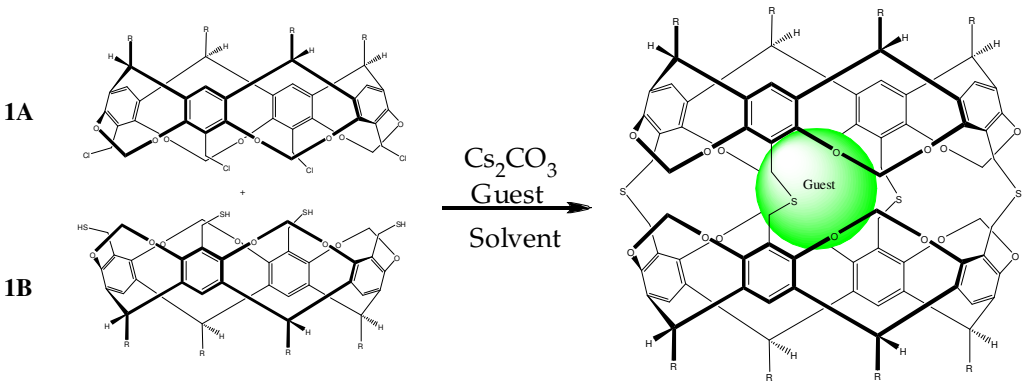

Figure 1. Synthesis of carceplex **2** from cavitands **1A** and **1B**.

Cram's subsequent research explored the construction and utilization of hemicarcerands[4] as molecular "reaction vessels" which is exemplified by the room temperature stabilization of highly unstable antiaromatic cyclobutadiene inside a hemicarcerand (Figure 2). Cyclobutadiene is otherwise fleeting and is only stable if frozen under cryogenic conditions in an inert gas matrix.[5] A solution of α-pyrone and empty hemicarcerand was heated, whereby one α-pyrone entered the inner cavity. Subsequently, the α-pyrone hemicarceplex was irradiated to induce the photochemical transformation of α-pyrone **3** into cyclobutadiene **5** via the intermediate photopyrone **4**. Extended irradiation resulted in the photochemical fragmentation of **5** into two molecules of acetylene which are small enough to escape the host hemicarcerand. This successful photochemical synthesis of encapsulated cyclobutadiene is the first reported reaction to be carried out in the inner phase of a hemicarcerand. Cram's 'taming of cyclobutadiene' is truly remarkable considering the high reactivity of **5,** which dimerizes in solution immediately to yield **6**.

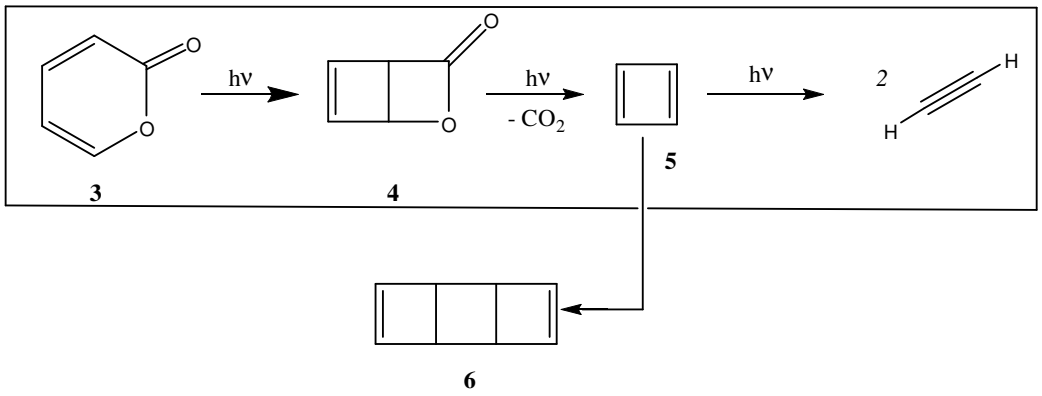

Figure 2. Photochemical pathway yielding cyclobutadiene.

The synthesis of most carcerands and hemicarcerands is low yielding due to the kinetic nature of the final assembly step. However, Fujita described two- and three-dimensional assemblies utilizing labile metal-ligand interactions and rigid building blocks that self-assemble under thermodynamic control into nanocapsules in essentially quantitative yields.[6] These assemblies utilize the fixed coordination geometry of a metal such as square planar Pd(II) and do not need the assistance of templating molecules. *cis*-Protection of Pd(II) with ethylenediamne produces **7** with 90° coordination geometry, which when coupled with tridentate ligand **8** in a 3:2 ratio yields the molecular octahedron **9** (Figure 3). Fujita's research demonstrates the power of using labile bonds, whose formation is under thermodynamic control for the multi-component synthesis of nanometer size molecular capsules.

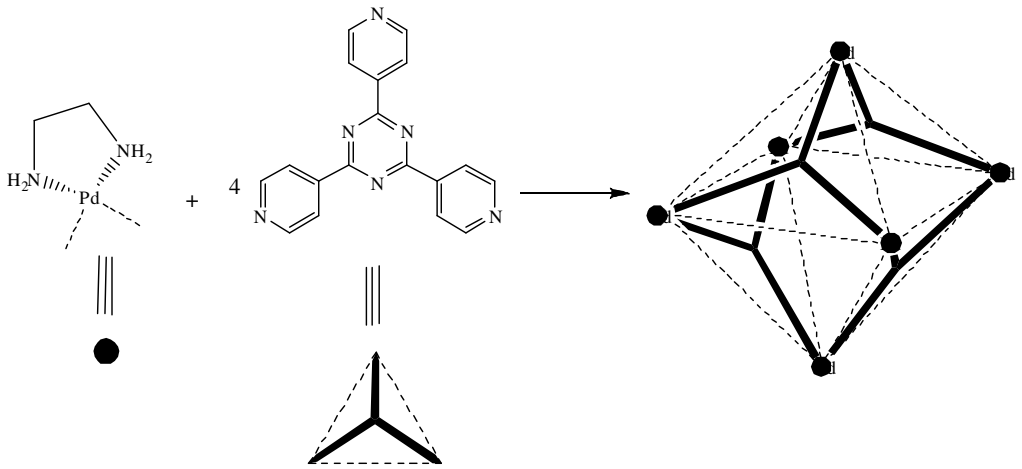

Figure 3. Octahedral assembly of *cis*-protected Pd(II) **7** and tridentate ligand **8**

The covalent equivalent of synthesis utilizing coordination bonds is dynamic covalent chemistry (DCC). An example of a dynamic covalent bond is the imine bond which forms upon condensation of an aldehyde or ketone and a primary amine. DCC makes use of reversible covalent bonds and imine bond formation has been used in reversible multicomponent synthesis.[7] The advantages of thermodynamically controlled synthesis are outlined in Figure 4. Assume (**A**) is the reactant and (**B**) the desired thermodynamic product. Even though (**A**) will initially form the less stable kinetic product (**C**), the latter will be eventually converted to the thermodynamically favored (**B**). Due to the reversibility of bond formation the final product is not governed by the relative transition state energies ($\Delta\Delta G^{\ddagger}$), but the relative stabilities of the reaction products ($\Delta\Delta G$).

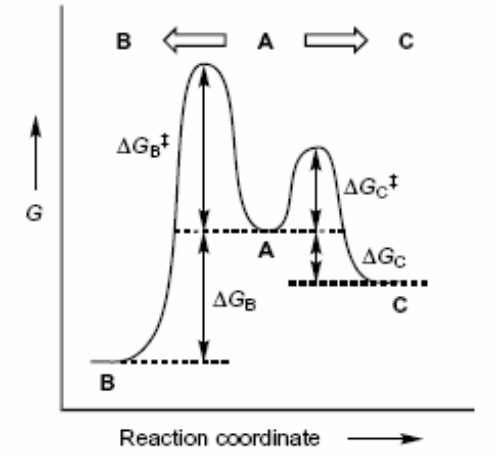

Figure 4. Free energy diagram illustrating kinetic vs. thermodynamic control of product formation.[8]

Cram successfully applied DCC in the synthesis of an octamine hemicarcerand where thermodynamic control of imine bond formation was demonstrated.[9] This work captures the essence of Fujita's approach; the rigid building blocks are two cavitands and four diamines and the thermodynamically labile bond is the reversible covalent imine bond (Figure 5).

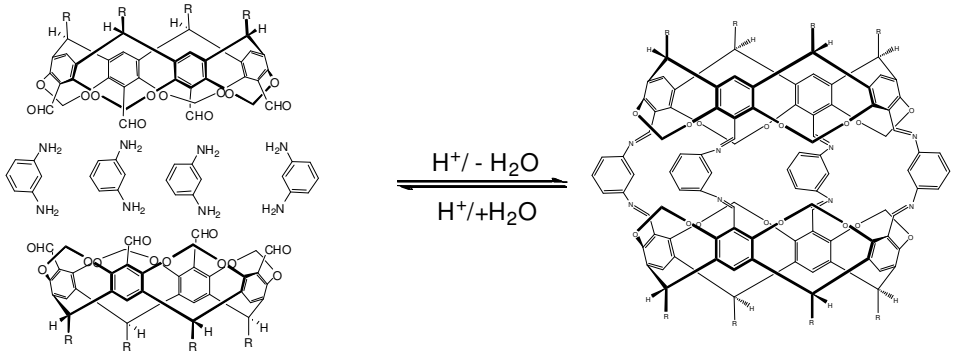

Figure 5. Assembly of two tetraformyl cavitands with *m*-diaminobenzene

More recently, DCC has been applied in the synthesis of an octahedral nanocontainer, which was assembled from six tetraformyl cavitands and twelve ethylenediamines in 80% yield.[11] This one-pot reaction (Figure 6) collected eighteen molecules in twenty-four bond forming reactions producing a nanocontainer which has a reported interior volume of 1700 Å^3.

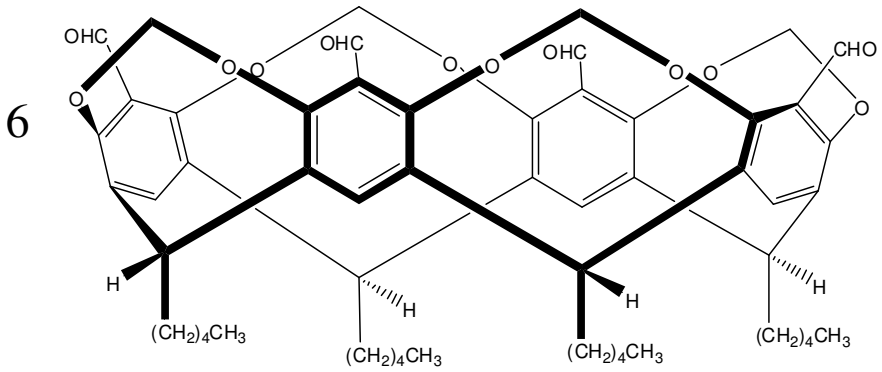

10

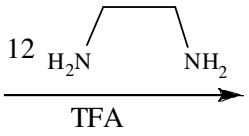

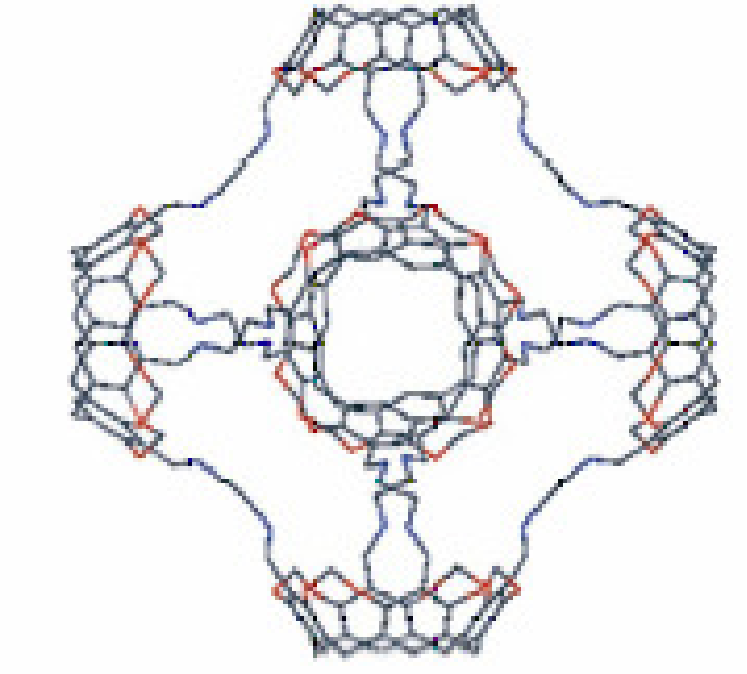

11

Figure 6. Synthesis of an octahedral nanocontainer using DCC.[11]
(Feet omitted for clarity). Structure **11** courtesy Dr. Ralf Warmuth.

CHAPTER 2

Focus of Research

Multicomponent assembly of tetraformyl cavitands into nanocontainers is successful owning, in part, to the rigidity of the cavitand building unit which ensures the four 'Y' moieties (Figure 7) are held inflexibly and symmetrically opposed; see the crystal structure for methylene spanned cavitand in Figure 8 (Y = Br). Previous work outlined in the introduction (Figure 6) focused on cavitand **10** with X = -CH_2-, which provided a rigid organic building block with C_4 symmetrically opposed 'Y' functionality. Condensation of **10** with ethylenediamine produced an octahedral nonocontainer.

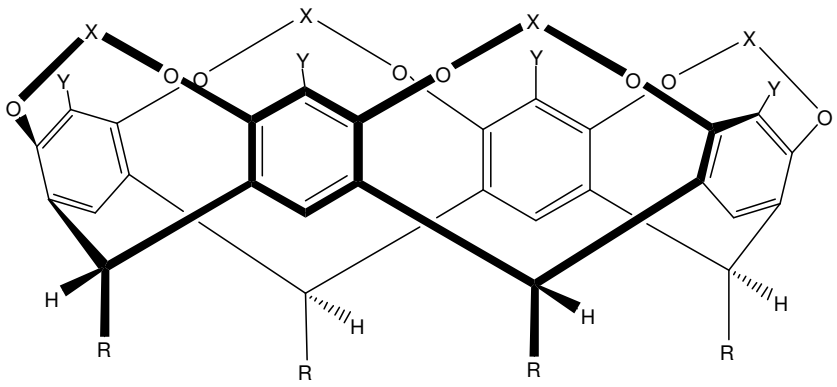

Figure 7. A cavitand with generic descriptors X ('spanner'), R ('feet') and Y

	Methylene Spanner	Ethylene Spanner	Propylene Spanner
Cavitand	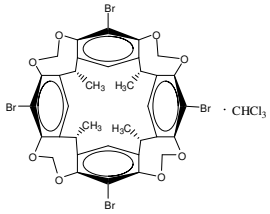	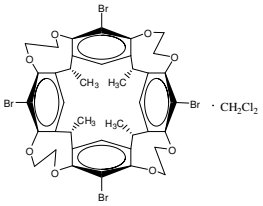	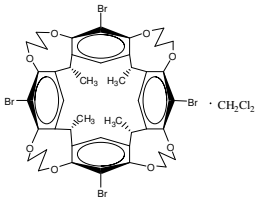
Crystal Structure[20]		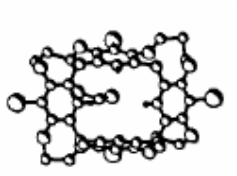	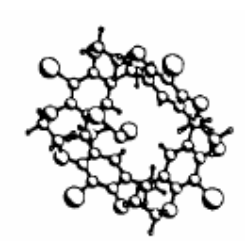
	12	**13**	**14**
Intra-cavity Br –Br Distance (Å)	9.34 x 9.81	9.77 x 12.53	8.16 x 13.57

Figure 8. Comparison of cavitands with different spanners including crystal structures.[12]

Related condensation reactions of cavitands with ethylene (**13**) and propylene (**14**) spanners have not been reported. Cavitands containing these spanners have cavity shapes that are different from that of cavitands with methylene spanners (**12**, crystal structures; Figure 8).[12] In crystal structures of **13** and **14,** the intra-cavity Br-Br distances are significantly less symmetrical leading to rectangular shaped cavitands with C_{2v} symmetry (bottom view; the large sphere 'bromides' are furthest from the

viewer). Furthermore, two opposing aryl rings are nearly vertical whereas the other two splay outward to a degree greater in **14** than is observed in **13**. However, these crystal structures, even though they may represent the lowest energy molecular conformation, may not represent the conformation adopted in a hemicarcerand or larger multicomponent nanocapsule.

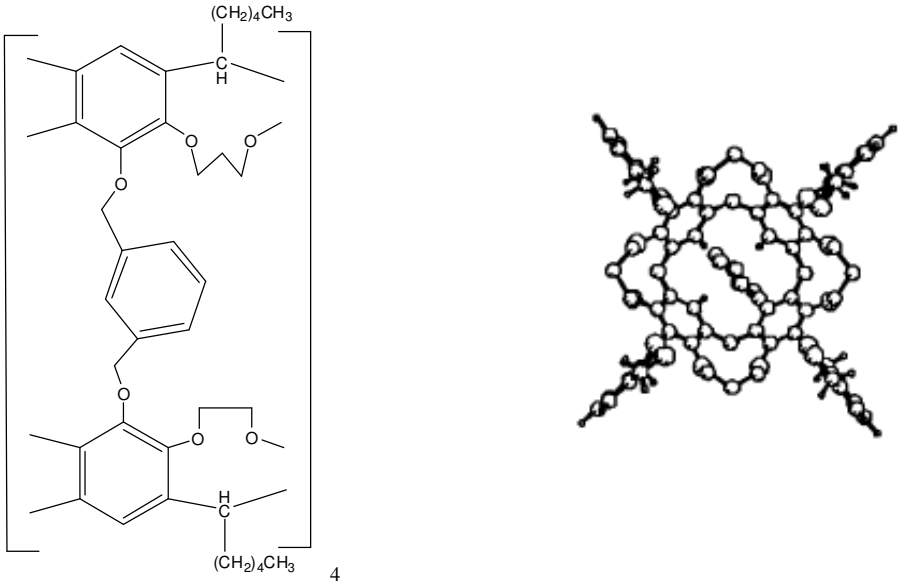

Figure 9. (L) mixed hemicarcerand. (R) partial crystal structure.[19]

For example, Cram reported mixed **PE** hemicarcerands & hemicareplexes,[19] which are composed of one propylene bridged cavitand and one ethylene bridged cavitand (see Figure 9; left). This **PE** hemicarcerand was subsequently complexed with 4-$CH_3C_6H_4OCH_3$ and the crystal structure was determined (right figure; Figure 9). Despite that the propylene and ethylene bridged cavitands as discussed earlier both adopt a rectangular shaped conformation, in the **PE** hemicarcerand the propylene

bridged cavitand has nearly perfect C_{4v} symmetry (Figure 9; right; top view; omits lower ethylene bridged cavitand). In fact, the dimensions for the cavity are 10.29 Å x 10.40 Å. Furthermore, the angles between opposing aryl units in both cavitands are nearly 90°. This suggests that a propylene bridged or ethylene bridged cavitands with 4 formyl groups (Y = CHO, X = $-CH_2CH_2-$ or $-(CH_2)_3-$ in Figure 7) may serve as a perfect corner piece for an octahedral nanocontainer. Thus, condensation of six propylene cavitands with twelve linear diamine spacers, such as ethylenediamine or 1,4-phenylenediamine, may form a nanometer sized octahedron in yields that are higher than those for cavitand **10** gave **11** in 80% yield. Two opposing aryl units form a ~60° angle in cavitand **10**. The design principles are outlined in Figure 10. An octahedron may be visualized as two regular four sided pyramids that share a common base and further contains six equivalent vertices.[13] Expressing this shape molecularly requires a tetratopic building block, which contains adjacent arms that form a 90° angle and neighboring arms form a 60° angle. Six of these tetratopic building blocks occupy the six vertices and are connected with 12 linear spacers along the edge of the octahedron. As detailed above, tetraformyl propyl-cavitand may be such an ideal 90° tetratopic unit.

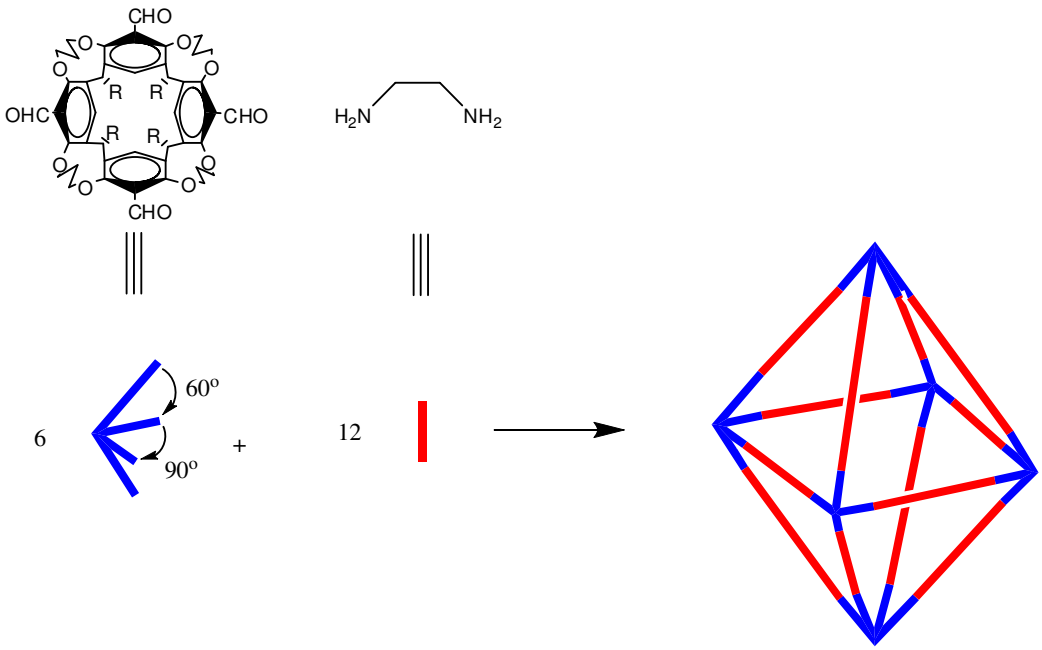

Figure 10. Conceptual presentation for octahedral shaped assembly using a linear ditopic spacer (red) and tetratopic corners (blue).

Furthermore, the spacer group is a critical parameter in this octahedral synthesis. According to the design principle above, a linear diamine spacer must be used and increasing the length of the diamine spacer beyond ethylenediamine will produce an octahedron with an interior volume larger than that of **11**. Molecular containers with large cavities are needed for the use of containers for drug delivery, in sequestration or storage of large numbers of molecules or the protection of a large molecule or cluster; e.g. could a metal nanoparticle be encapsulated and protected from an oxidizing environment? Figure 11 identifies some reasonable spacer candidates that meet the criteria for rigidity, correct functionalization and molecular size.

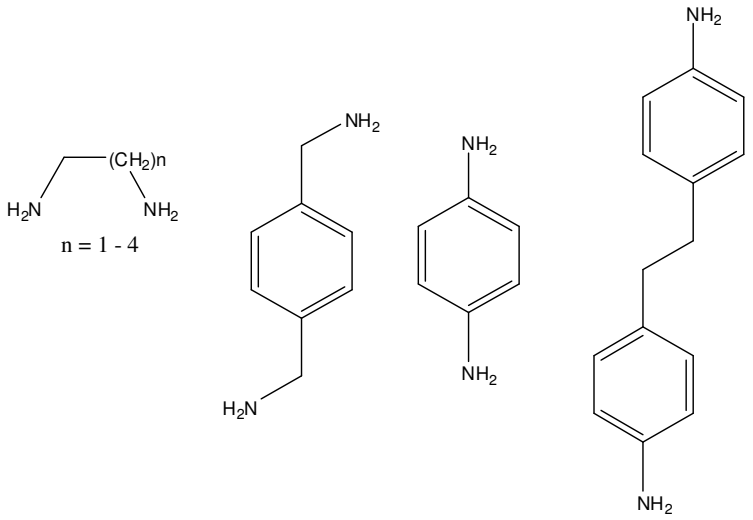

Figure 11. Possible ditopic spacers for self-assembly.

The regular shaped cavity of **10** condenses with ethylendiamine to produce an octahedral assembly in 80% yield.[11] In different solvents a tetrameric product as well as an octameric product[10] was formed with the same reactants. The knowledge gained from the condensation reactions of **10** should allow for successful investigation of the propensity of cavitands with ethylene and propylene spanners to form supramolecular assemblies.

CHAPTER 3

Experimental Results

3.1 Results: Formylation of Ethylene-Cavitand

Formylation of in-hand tetrabromide **15** was first attempted by application of a previously successful procedure for a methylene bridged cavitand. This procedure involves carefully drying the starting tetrabromide overnight at 120ºC under high vacuum. The flask containing the tetrabormide is flushed with Ar and dry THF is syringed in. After cooling the flask to -78ºC with a dry ice/acetone bath, n-BuLi is syringed in to perform a halogen-lithium exchange. The solution is stirred for 30 min and then a 0ºC bath replaces the -78ºC bath. Stirring continues for sixty additional minutes after which the solution is cooled to -78ºC and dry DMF is added. After 60 minutes has elapsed, the bath is removed and the flask is allowed to stir at room temperature for an additional 60 minutes. The flask contains a suspension of the anionic intermediate **III** (see figure 13) which is quenched with a 5% aqueous solution of NH_4Cl.

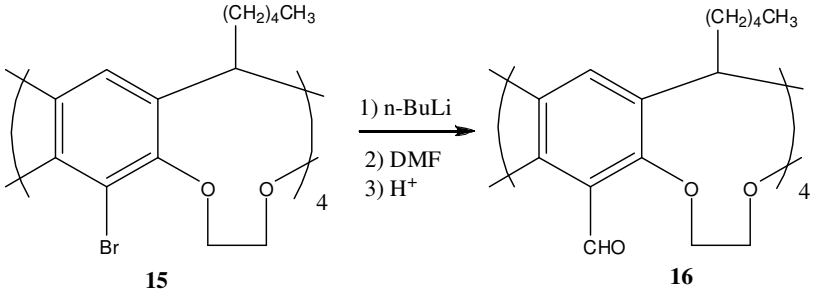

Figure 12. Proposed method for formylation of ethylene bridged cavitand **15**.

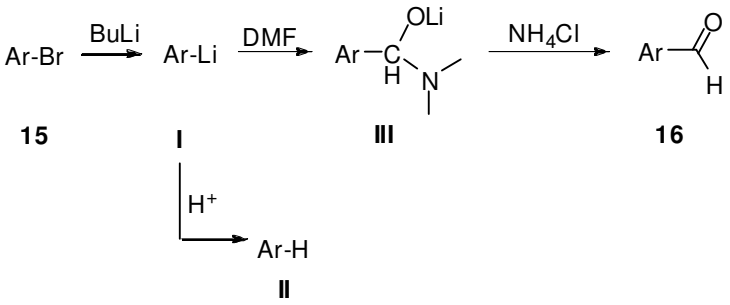

Figure 13. Scheme of formylation for **15**.

The initial attempt to formylate **15** with the aforementioned method yielded significant protonation. Examining the ^{1}H-NMR spectrum of the products at around δ 7.2 ppm shows that the initial halogen-metal exchange was successful as evidenced by the lack of peak **A** (para-proton to bromide) in the bottom spectrum (figure 14). However, the anion was quenched by a proton as evidenced by the presence of peak **B** at δ 6.7 ppm in the bottom spectrum. The ratio of the peaks at δ 6.7 ppm and the formyl peaks (10.3 -10.4 ppm) yields 30% protonation. With this degree of protonation, the statistical yield of the tetraformyl cavitand **16** is $(0.7)^4$ or 24%, which is too low considering the difficulties to separate the desired cavitand from side products.

Determining where in the reaction sequence the proton source was being introduced is paramount and it was speculated that DMF was the culprit because it is

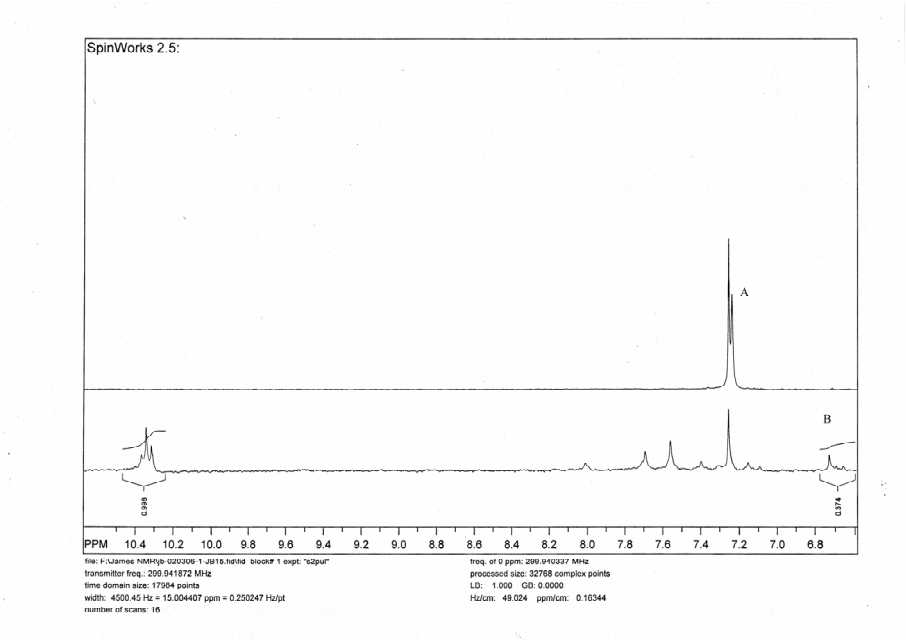

Figure 14. Partial ^{1}H NMR (400MHz, $CDCl_3$, 296K). Top: Tetrabromide **15**; Bottom: crude formylation product

known to undergo degradation in storage.[13] Thus, a metal-halogen exchange was performed of **15** and D_2O was added to quench the reaction mixture. The results indicated that DMF was not the [only] culprit and protonation (**II**) was taking place prior to addition of the electrophile (Figure 15). Thus, it was suspected that water was introduced with the reaction solvent, THF. After it was ensured that the THF was completely dry, quenching with D_2O yielded clean, quantitative proton/deuteron exchange (Figure 16).

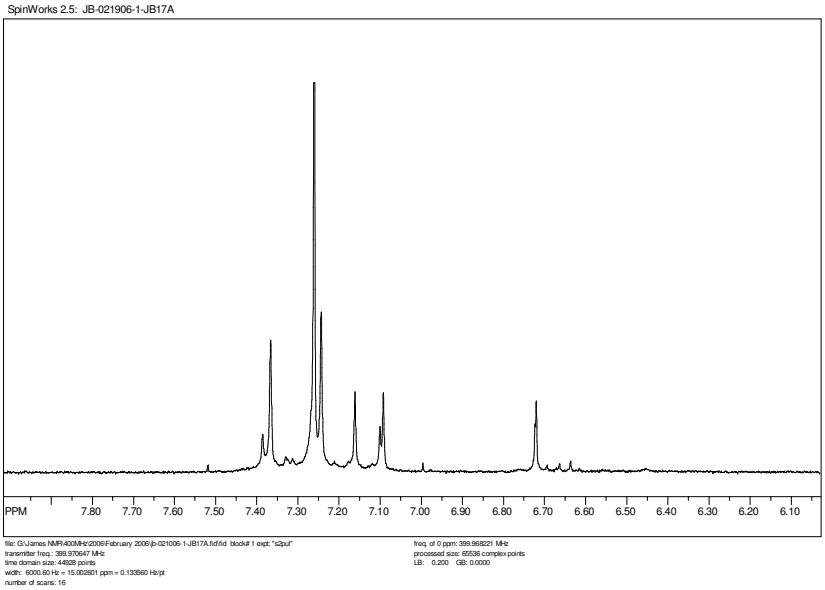

Figure 15. ^{1}H NMR, Results of the D2O quenching products of the Br/Li exchanged products of **15**. (400MHz, $CDCl_3$, 296K)

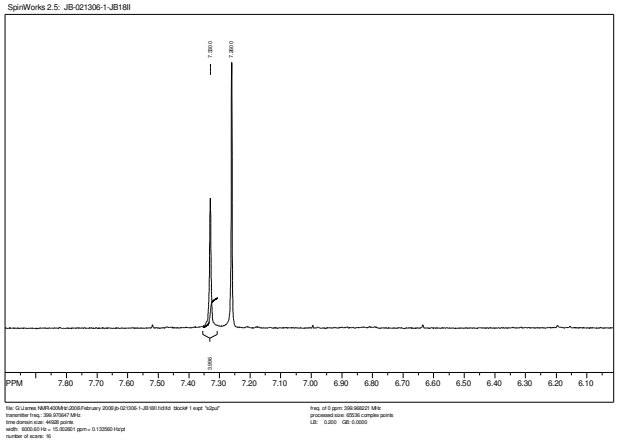

Figure 16. ^{1}H NMR, D_2O quenching results after careful drying of solvent THF; δ 7.33ppm: aryl proton *para* to deuteron. (400MHz, $CDCl_3$, 296K).

Formylation of **15** was attempted now that it appeared that the reaction conditions were under control. Unfortunately, 47% protonation was still observed (Figure 17) by integration which provides a statistical yield of 8% for **16**.

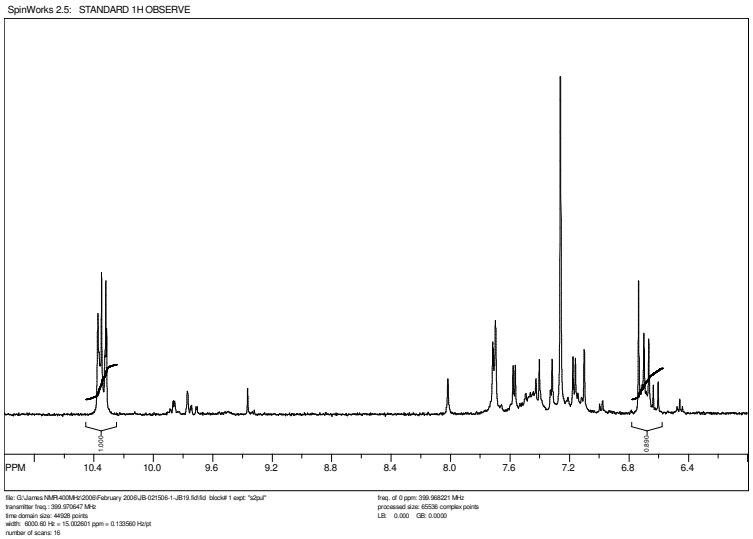

Figure 17. Partial ^{1}H NMR (400MHz, $CDCl_3$, 296K) of crude products of a formylation of **15**.

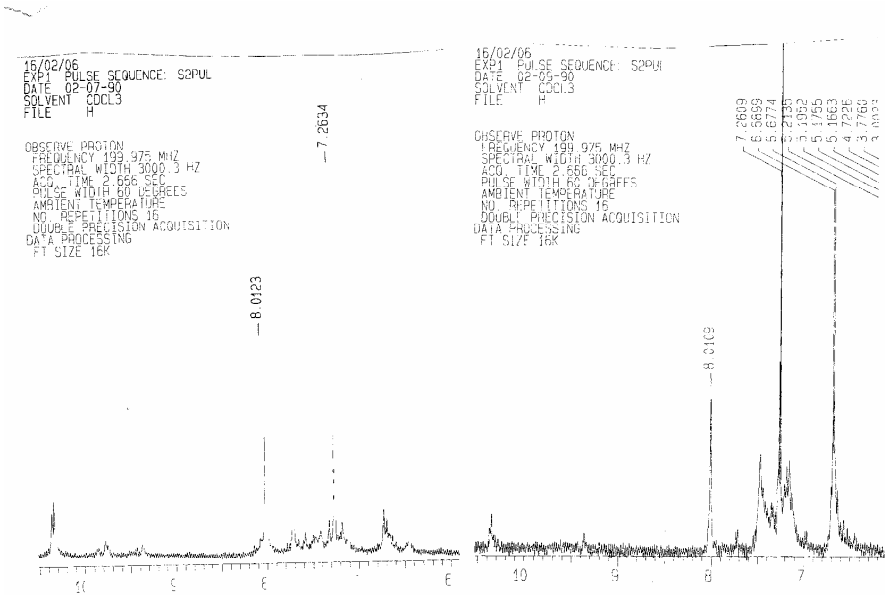

Figure 18. Partial ^{1}H NMR (200MHz, $CDCl_3$, 296K) spectrum of crude products of the formylation of **15**. Left spectrum: 3 hr reaction time; Right spectrum: 24 hrs. reaction time

To get more insight into the source of protons, a Br/Li exchange was performed as described before. Subsequently, DMF was added at -78°C and the reaction mixture was left stirring for 24 hours at -78°C. Two samples were taken after 3 hours and 24 hours and were immediately quenched with H_2O. The left partial spectrum of Figure 18 shows the reaction composition after 3 hours and the right partial spectrum shows the same reaction after 20 hours. The metal-halogen exchange is complete. After 24 hours protonation predominately occurred, but the ratio of formylated to protonated aryl groups has decreased drastically over this time period. This behavior was not expected to occur. Thus, the ArLi (**I**) is slowly protonated through an external source, prior to the addition of DMF. Therefore, more reactive electrophiles such as methyl formate and phenyl formate were tested in the hope that they would quench **I** before it is protonated. The ^{1}H-NMR spectrum of the crude products of the metalation of **15** and subsequent exposure to methyl formate as electrophile is shown in Figure 19. Again, protonation is 51% by integration which gives a statistical yield of 5.8% for **16**. The last electrophile employed in an attempt to formylate **15** was phenyl formate. The ^{1}H-NMR spectrum of the products (Figure 20) shows 45% protonation by integration which gives a statistical yield of 9.2% for **16**. Factors beyond simple solvent impurities seem to be at play with this reaction.

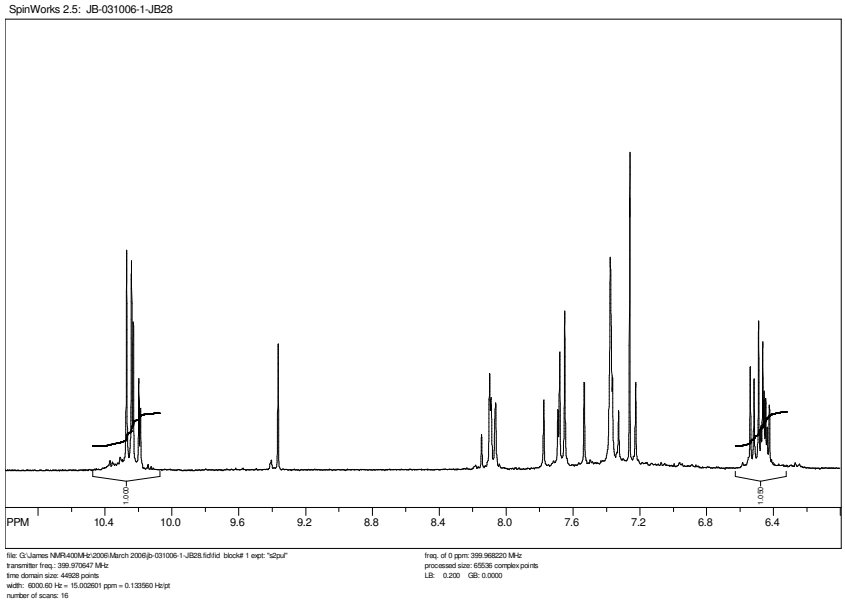

Figure 19. Partial ^{1}H-NMR(400MHz, $CDCl_3$, 296K) of the products of the formylation of cavitand **15** with methyl formate.

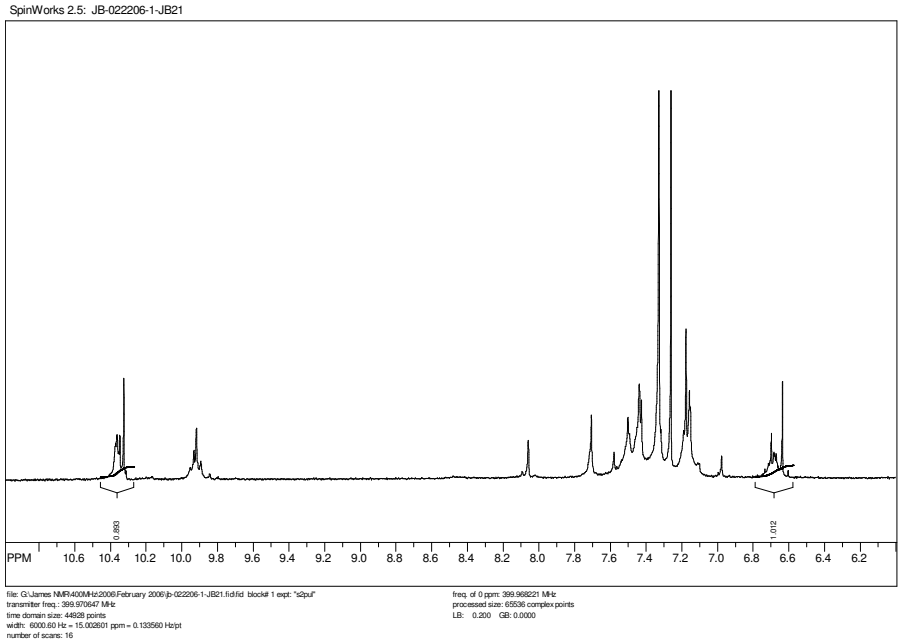

Figure 20. Partial ^{1}H-NMR(400MHz, $CDCl_3$, 296K) of the products of the formylation of cavitand **15** with phenyl formate.

3.2 Formylation of Ethylene-Cavitand

The behavior of **15** in the formylation reaction is explained as follows. Metal-halogen exchange for cavitand **15** is successful as demonstrated in Figure 16 in which complete deuterium incorporation was observed in the ^{1}H NMR. However, protonation was observed during the addition of electrophiles DMF and methyl formate.

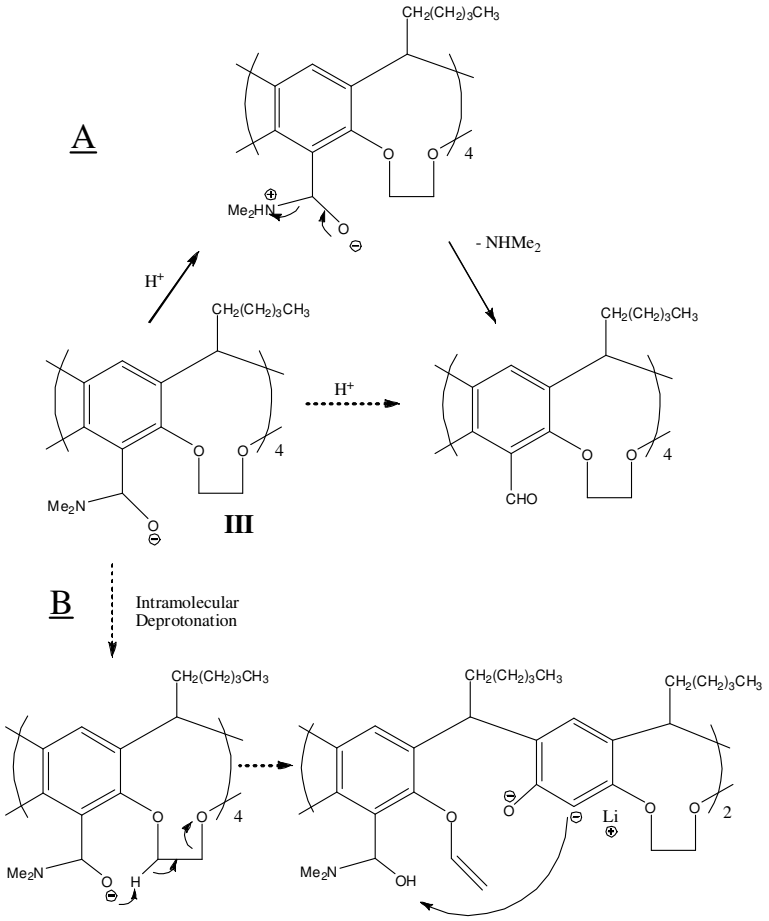

Figure 21. Pathway A: Desired pathway which produces a formyl group.
Pathway B: Suggested pathway for protonation.

After lithiation of cavitand **15**, nucleophilic attack on DMF yields an anionic intermediate (**III**), which collapses with the loss of dimethylamine upon addition of acid in the last step of the sequence, as demonstrated by reaction pathway **A** in Figure 21. In pathway **B**, the amino alkoxide acts as an intramolecular base catalyzing the β-elimation reaction of an ethylene spanner. Subsequently, the carbinolamine quenches an unreacted ArLi. Examining an energy minimized structure of the tetra-anionic intermediates (Figure 22), demonstrates a close spatial relationship between alkoxide and one spanner proton.

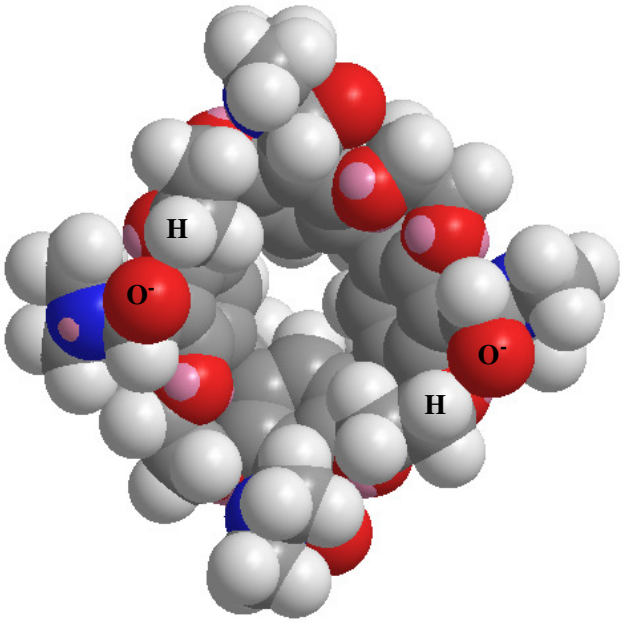

Figure 22. View into the cavity of intermediate tetra-anion for formylation of **15**.

Intramolecular deprotonation may be possible with Li being coordinated to the alkoxide anion. However, deprotonation will certainly be accelerated by the addition of DMF, which breaks up ion pairing of the Li-alkoxide. This deprotonation then

yields a sufficiently acidic proton which can quench the aryl anion. The vinyl ether functionality is lost during acidic workup of the reaction. β-Elimination should not take place in a propylene-cavitand, thus the formylation reaction was studied for cavitand **18**.

3.3 Results. Formylation of Propylene-Cavitand Using BuLi

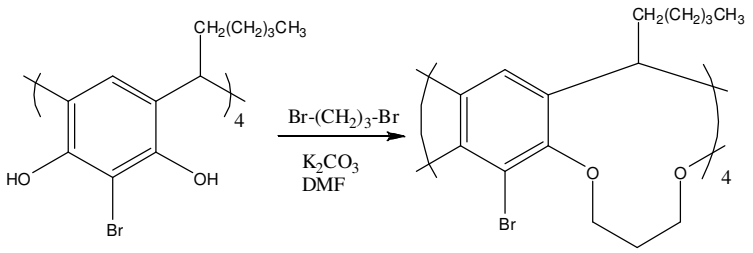

17 **18**

Figure 23. Synthesis of propylene bridged cavitand **18** from bromo-octol **17**.

Cavitand **18** was successfully synthesized from bromo-octol **17** in 45% yield according to a previously published procedure.[14]

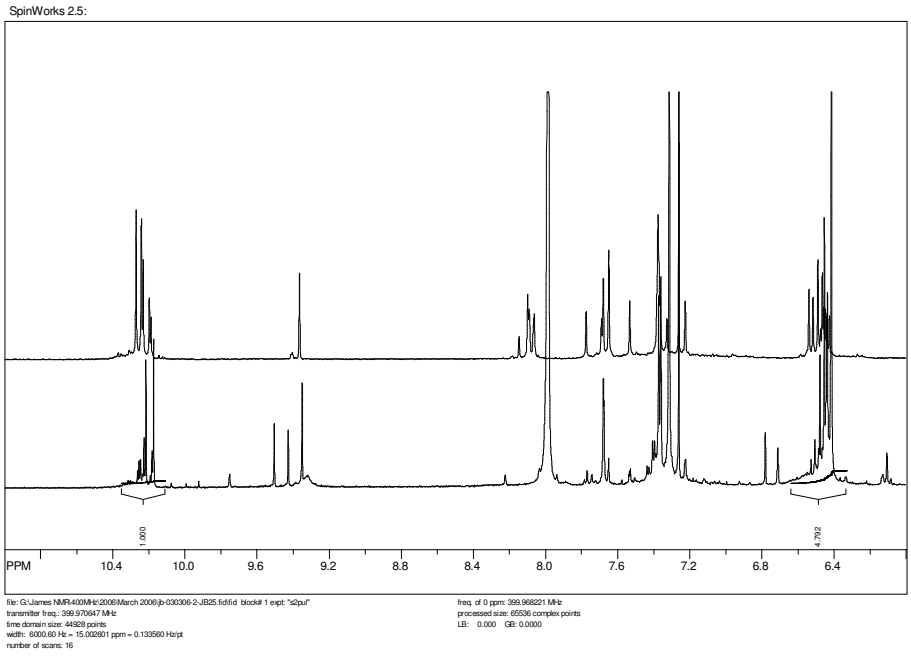

Figure 24. Partial ^{1}H-NMR (400MHz, $CDCl_3$, 296K).of the crude reaction products of formylation reactions of **18**. Top: methyl formate as electrophile; Bottom: DMF as electrophile

After synthesis of cavitand **18**, formylation was attempted using DMF and methyl formate in two separate experiments using the previously described method. Again incomplete formylation was obtained using DMF as the electrophile, with 82% proton incorporation, or a 0.1% statistical yield of **18**. Using methyl formate as electrophile yielded 51% proton incorporation, or 5.8% of **18**. At this point, it seemed prudent to check the metalation reaction for protonation before the electrophile is added, considering previous attempts to synthesize **16**.

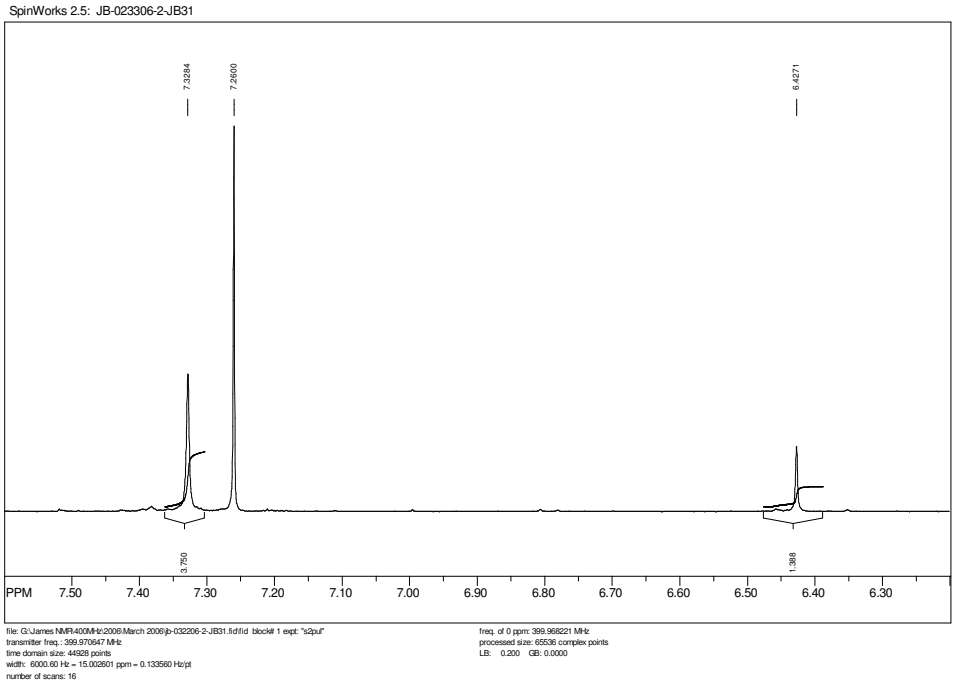

Figure 25. Partial ^{1}H-NMR (400MHz, $CDCl_3$, 296K) for the metalation of **18** followed by D_2O quenching.

Testing for the effectiveness of the metal-halogen exchange reaction for cavitand **18** involved trapping with D_2O. Any proton incorporation must be from solvent or reagents other than DMF as it was not introduced. The ^{1}H-NMR spectrum of the reaction products (Figure 25) show that the metal-halogen exchange is complete by the lack of any aryl proton at δ 7.07 ppm, but protonation has occurred as evidenced

by the singlet at δ 6.43 ppm. Integration of the peaks at δ 6.43 ppm and δ 7.33 ppm should yield a 1:1 ratio, but instead a ratio of 2.7:1 (7.33 ppm : 6.43 ppm) is found. This indicates that the ^{1}H NMR silent deuterium was incorporated, but a significant amount of protons are being incorporated from either the solvent or the reagents. The reaction was modified by using t-BuLi in place of n-BuLi and the metalation/D_2O quenching experiment was repeated. Twenty minutes after a -78ºC solution of **18** in THF was treated with t-BuLi a sample was removed and immediately quenched into D_2O. Methyl formate was added next, and stirring continued at -78ºC for three hours and the reaction was quenched with D_2O. The twenty minute sample (Figure 26) shows much less proton incorporation than previously observed. The metal-halogen exchange is complete because of the absence of any peak at 7.07 ppm. The aryl peak at 7.33 ppm is roughly twelve times greater than the peak at 6.42 ppm, which indicates significant deuterium incorporation.

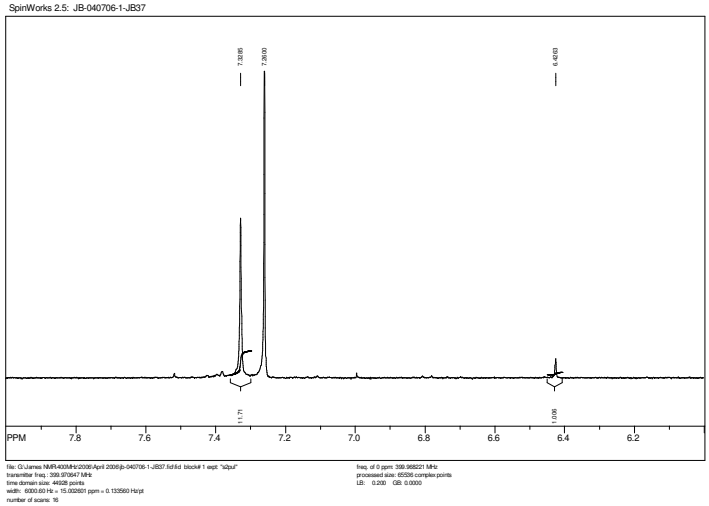

Figure 26. Partial ^{1}H-NMR (400MHz, $CDCl_3$, 296K) spectrum of products of the -78ºC metal-halogen exchange of **18** with t-BuLi after 20 minute reaction time followed by quench with D_2O.

Unfortunately, addition of methyl formate and subsequent reaction at -78ºC still yields 52% protonation by integration. This leads to a 5.3% statistical yield of **19**.

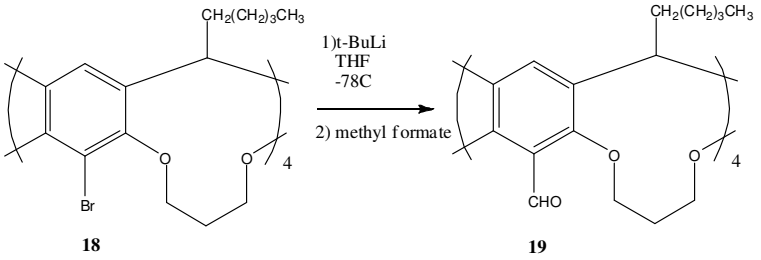

18 **19**

Figure 27. Formylation of **18** using t-BuLi and methyl formate.

The shortened reaction time seems to stave off the protonation process without sacrificing the efficiency of the metal-halogen exchange, but any gain in the exchange is lost because the rate of protonation is greater then addition of methyl formate at the reactive site.

3.4. Discussion: Formylation of Propylene-Cavitand Using BuLi

Formylation of cavitand **18** using lithium chemistry for the initial metal-halogen exchange fails because of significant protonation. Cavitand **18** has a slot shaped cavity, which is complementary to the shape of THF. The cavity may hold THF in an orientation that allows for the aryl anion to abstract a proton from the solvent. β-elimination for THF is a known process.[18] Possibly, this mechanism yields protonation of **18** during metal-halogen exchange.

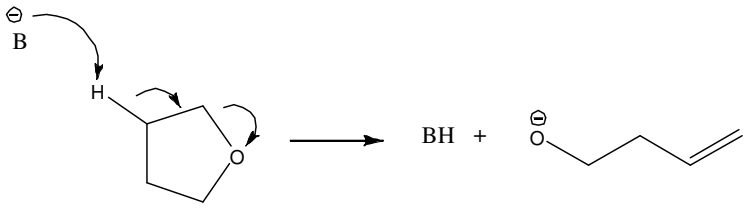

Figure 28. β-elimination of THF.

3.5 Results. Formylation of Propylene-Cavitand Using Grignard Reagent

In an attempt to eliminate the protonation side reaction, Grignard type reagents developed by Prof. Dr. Paul Knochel at Ludwig-Maximilians-Universität in München, Germany were applied. In particular, Knochel reports a complex of LiCl and i-PrMgCl that showed great utility in metal-halogen exchange reactions.[15] Knochel attributes a rate increase in metal-halogen exchange to the breaking up of *i*PrMgCl polymeric aggregates by lithium (evidenced by the need for stoichiometric amounts of LiCl) producing a more reactive iPrMgCl$_2$Li monomer. The Grignard reaction of **18** using this reagent is slow at low temperatures but at room temperature complete metal-bromide exchange took place. After quenching with DMF, successful formylation of **18** could be achieved to give **19** in 45% yield.

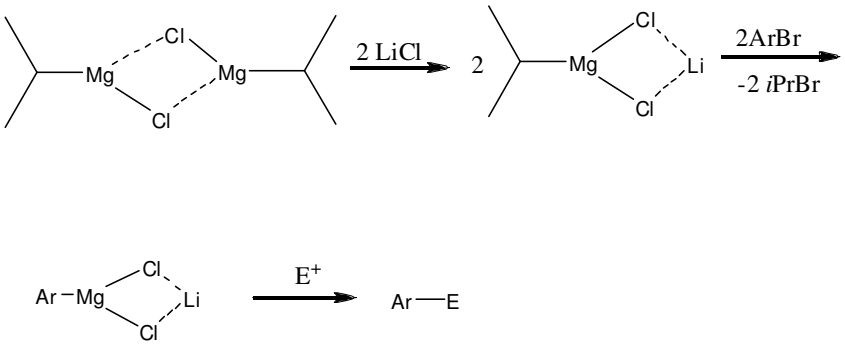

Figure 29. Knochel's proposed mechanism: *i*-PrMgCl·LiCl.[15]

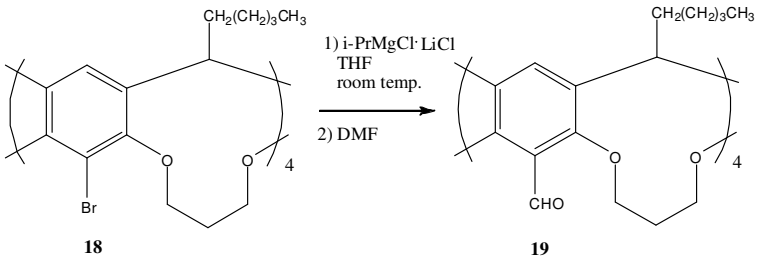

Figure 30. Successful method for formylation of cavitand **18**.

Tetraformyl cavitand **19** was recrystallized from 1:1 hexanes:$CHCl_3$ by layering of hexanes over a saturated solution of **19** in $CHCl_3$ and cooling. Nearly colorless needles of **19** were recovered after crystallization and submitted for x-ray crystallographic analysis. The x-ray structure shows that two molecules of **19** crystallize with six $CHCl_3$ molecules in the unit cell, which has space group P-1 (Figure 31). The unit cell dimensions are: a = 14.5817Å, b = 15.5718 Å, and c = 16.7809 Å. The unit cell angles are α = 87.1230º, β = 75.457º, γ = 68.0350º, which yields a cell volume of 3416.46$Å^3$. It is interesting to note that the torsional angle between the formyl group and the flattened aryl ring is not 180º, but about 174º due to crowding by the spanner methylenes. Also, the outward splay of two aryl rings is visible in the x-ray structure (Figure 31) and is similar to that reported by Cram for the related tetrabromo-cavitand **14** (Figure 8).

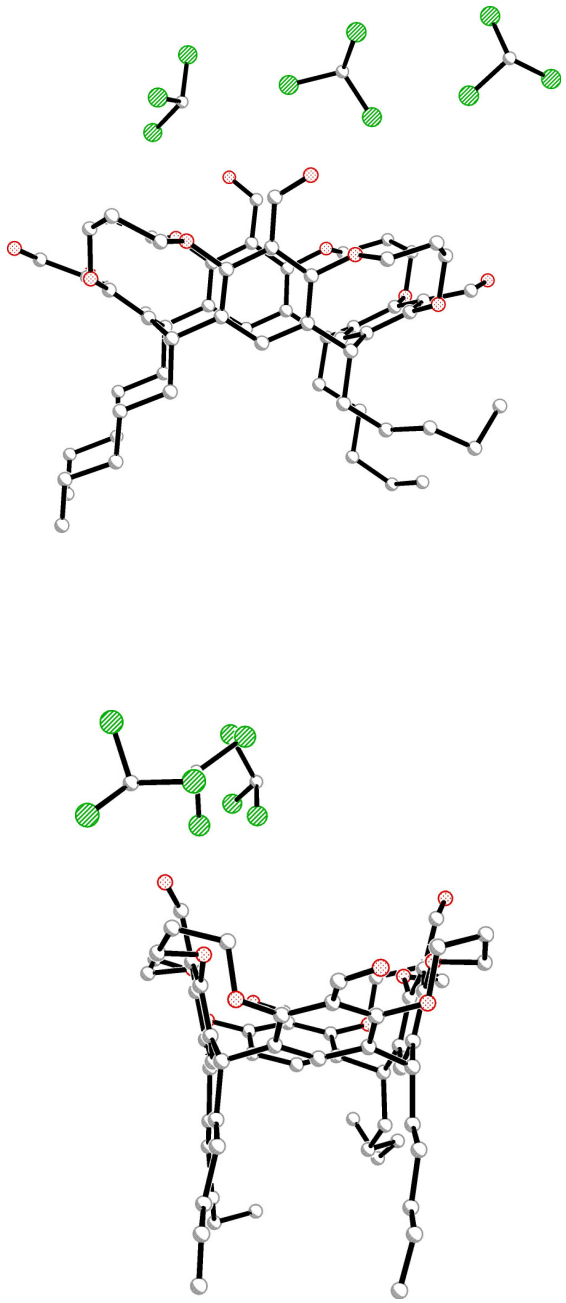

Figure 31. X-ray structure for **19**.

3.6. Results: Assembly of 19 Using Dynamic Covalent Chemistry

With tetraformyl cavitand **19** in hand, condensation reactions with various diamines were attempted. In consideration of the solubility of **19**, chloroform is an excellent choice of solvent, but care must be taken to remove any acid and moisture. Imine bond formation is a reversible process that is sensitive to water and catalyzed by acid. Generally, these reactions are most successful if stoichiometric amounts of reactants are used. After dissolution of the reactants, 1 mol% TFA is added. The solution is allowed to stand undisturbed under argon and the assembly process is monitored by size exclusion chromatography and NMR.

Condensation of **19** with the amines listed in Figure 32 resulted in complex product mixtures containing a majority of dicavitand products as determined from MALDI-TOF mass measurements. Optimization of these reactions to produce a single polycavitand product was unsuccessful.

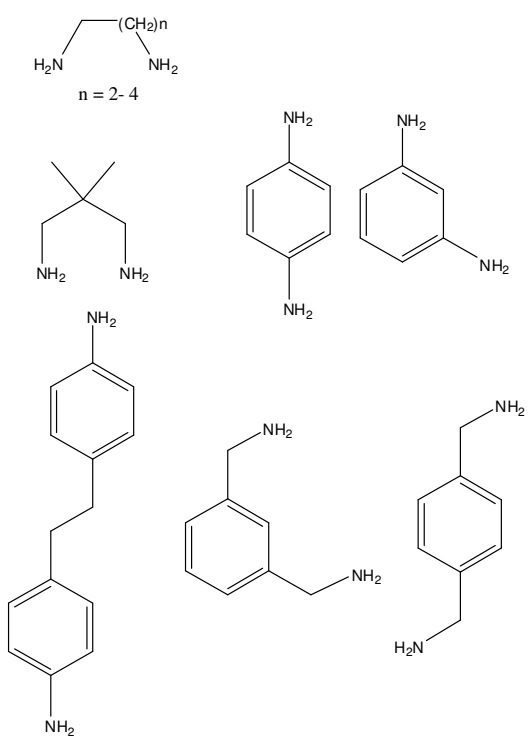

Figure 32. Amines that did not produce large assemblies.

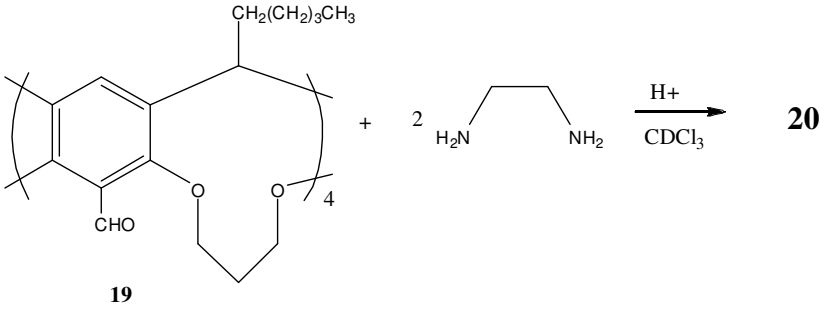

Figure 33. Condensation of **19** with ethylenediamine yielding tetramer **20**.

However, the condensation of **19** with ethylenediamine in stoichiometric amounts yielded a single product with m/z = 4360 [M + H^+], which is in good agreement with the calculated mass (m/z = 4357) for an assembly of four cavitands and eight ethylenediamine with complete formation of sixteen imine bonds. Figure 34 shows a partial ^{1}H-NMR spectrum. Four distinct broad singlets for the imine protons in a ratio of 1:1:1:1 are observed. Unfortunately, suitable crystals could not be obtained for x-ray crystallographic analysis.

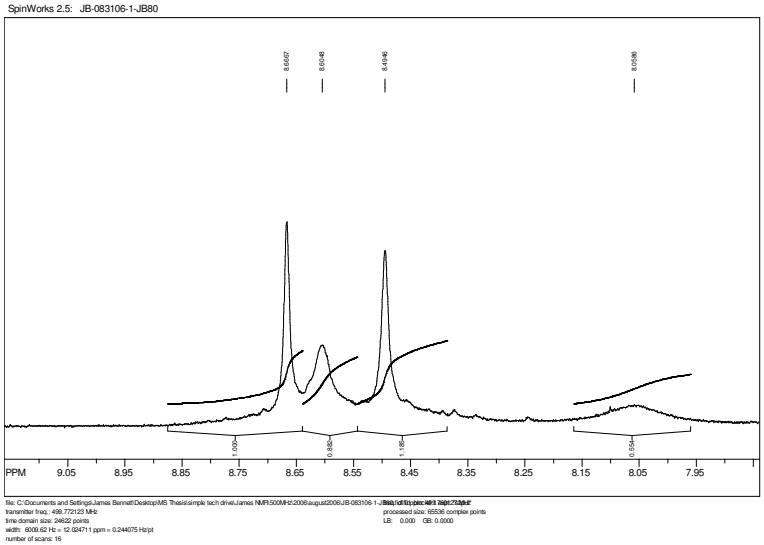

Figure 34. Partial ^{1}H-NMR (400MHz, $CDCl_3$, 296K) spectrum of the teteramer **20** showing distinct broad singlets for the imine protons.

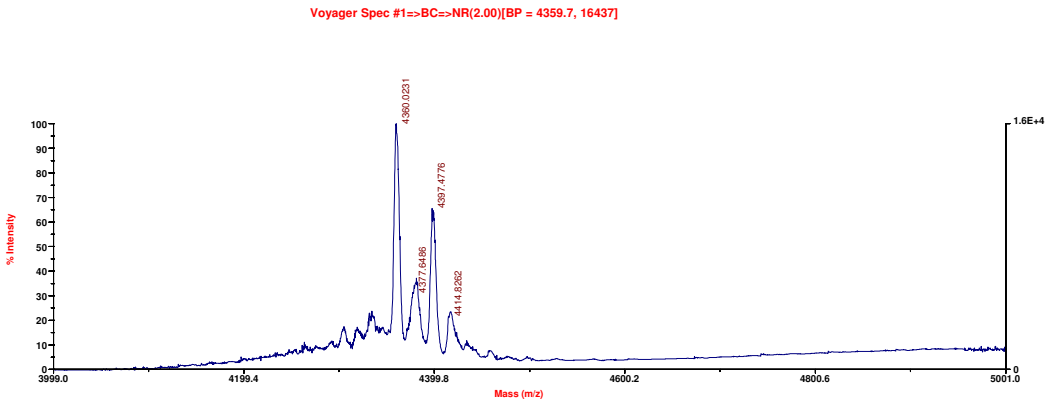

Figure 35. MALDI-TOF MS of **20**; 4360 [M+H^{+}]

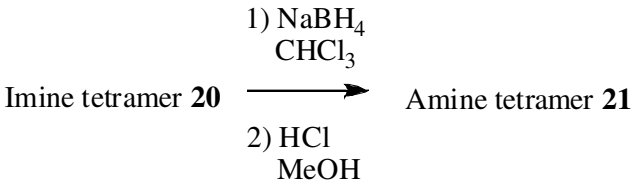

Figure 36. Reduction of imine tetramer **20** to amine tetramer **21**.

Reduction of all sixteen imine bonds in the tetramer **20** was possible with $NaBH_4$. Hydrolysis of the intermediate borane-nitrogen complex was very slow and did not go to completion at room temperature. Thus, after fully dissolving the intermediate in MeOH and careful addition of HCl (aq), the clear solution was refluxed until MALDI-TOF mass analysis showed complete hydrolysis (~five days). Again, suitable crystals could not be obtained for x-ray crystallographic analysis, which is needed to determine the structure of this tetrameric product.

3.7. Discussion: Assembly of Cavitand 19 Using Dynamic Covalent Chemistry

The condensation of tetraformyl cavitand **19** and ethylenediamine yields a teteramer **20,** which is composed of 4 cavitands and 8 diamines. From the ^{1}H-NMR spectrum of this molecule, the four unique imine protons observed in a 4:4:4:4 ratio in the 1H-NMR spectrum of **20** (Figure 34) suggesting a high degree of symmetry in the structure. The six highest symmetric structures that may results from the reaction of a tetratopic cavitand and a flexible diamine are depicted in Figure 37. In these structures, each circle represents a cavitand and each line a spacer. Structures **A**-**E** represent donut shaped rings. Structure **F** is a distorted tetrahedron in which two cavitand are doubly linked to each other in A/B position and singly to the remaining two cavitands. A unique feature of **B** - **E** is a twist (crossing of linkers). A single twist is present in molecule **B**, a double twist in **C** and **D** and a triple twist in **E**. One could even imagine a quadruple twisted strip (not shown). Donut-like structure **A** is highly symmetrical and would only show one imine in the ^{1}H-NMR spectrum. The same would be the case for the un-displayed quadruple twisted structure. Structure **B** is predicted to have six unique imine protons as does structure **E**. Structure **C** has three unique imine protons as does structure **F**. The most likely structure for **20** is **D**, which is double twisted and has four unique imine protons as observed in the ^{1}H-NMR spectrum of **20**. Furthermore, space-filling models of **D** show that four of the imine bonds are at the interior of the molecule (Figure 38). This would explain the slow rate of imine bond reduction and subsequent hydrolysis as well as the broadened and upfield shifted imine singlet observed at approximately 8 ppm.

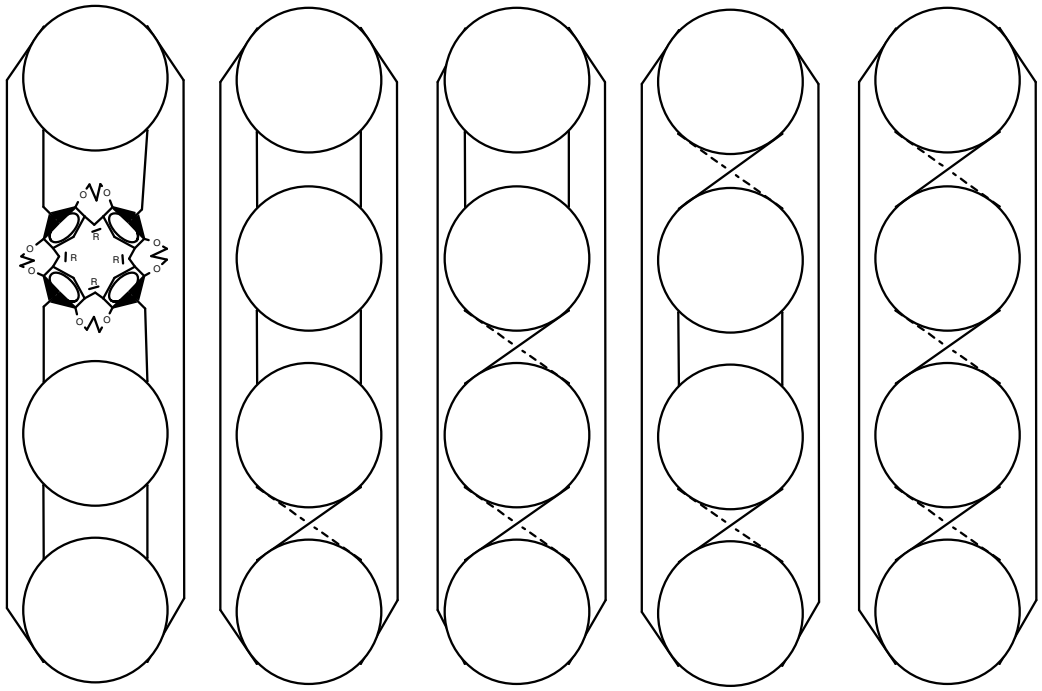

A B C D E

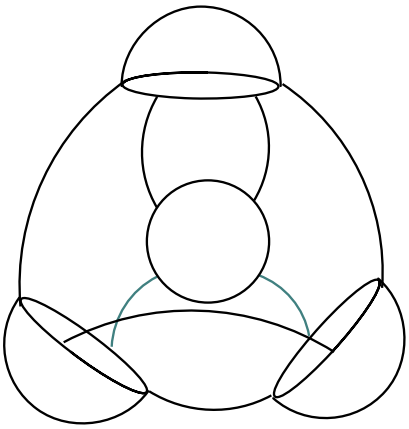

F

Figure 37. Possible structures for **20**

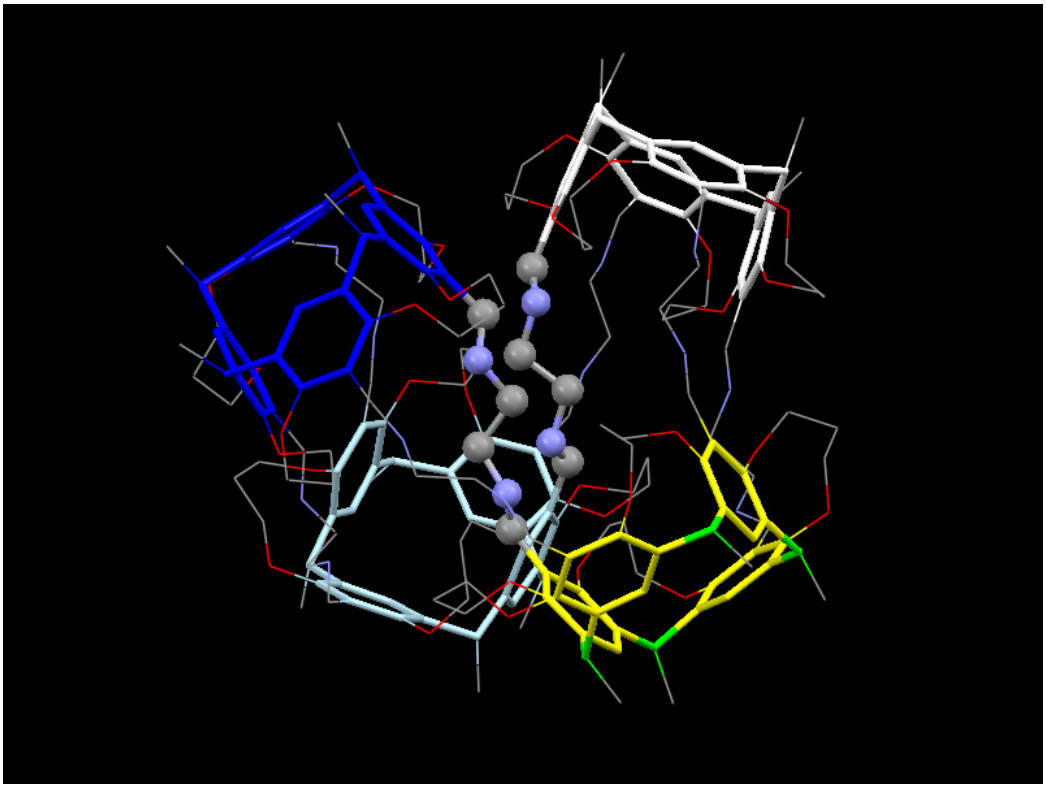

Figure 38. Space filling model of tetramer **D** highlighting four interior imine bonds.

3.8. Results: Dynamic Covalent Chemistry Assembly of Cavitand 19 Using Triamine 22

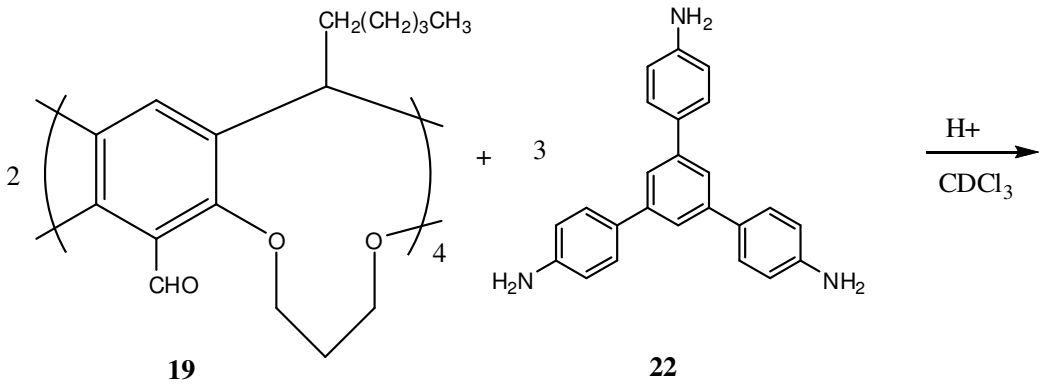

Figure 39. Condensation of triamine **22** with cavitand **19**.

The condensation of **19** with triamine **22** was also investigated. Earlier, it was shown in our laboratory that the condensation of rigid triamine **22** with **10** yields a hexameric nanocapsule.[16] Maintaining strict stoichiometry in this reaction was detrimental to the yield because of the dominate production of pentameric kinetic products that would not further equilibrate unless a large excess of **22,** which acts as a transimination catalyst, was present. Thus, when **22** was used in 50% excess, a hexameric structure similar to the product seen in scheme 5 was produced in excellent yield. It is postulated that initially formed large oligomers are broken down by **22** through a sequence of transimination reactions.[7] The condensation of **19** with **22** (50% excess) was studied in the hope of producing a similar hexameric product. The

reaction was followed by GPC (Figure 38). After two weeks a dominate peak formed at 11.56 minutes. The masses of ions detected in MALDI-TOF MS of this sample allowed for a correlation between the retention time of the dominate products and the assembly molecular weight and is shown in Figure 39.

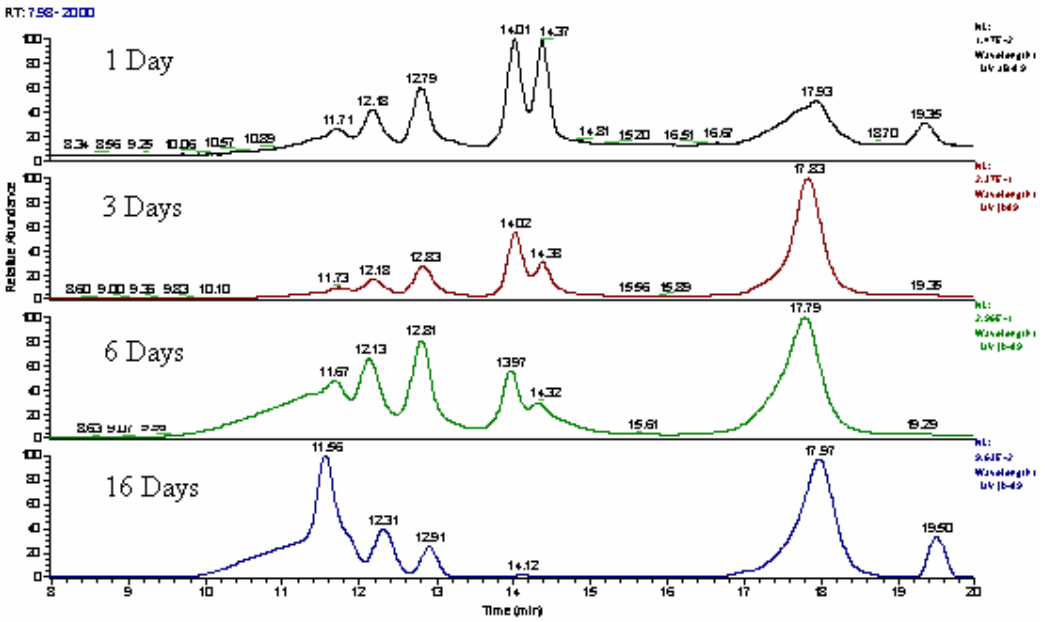

Figure 40. GPC for condensation **19** with **22** (50% excess).

In the MALDI-TOF MS in Figure 42, the largest ion has an m/z of 7697, which correlates with the mass of the $[M+K^+]^+$ ion of an assembly containing 5 cavitands and 8 triamine linkers that are linked together by 20 imine bonds.[17] This assembly has four unreacted amines which do not appear to undergo further reaction with a sixth cavitand given the lack of higher molecular weight ions. Also, a fully formed hexameric assembly is not present as indicated by the absence of ions $[M + H]^+$ with

the expected m/z 8625 in the MALDI-TOF (Figure 40).

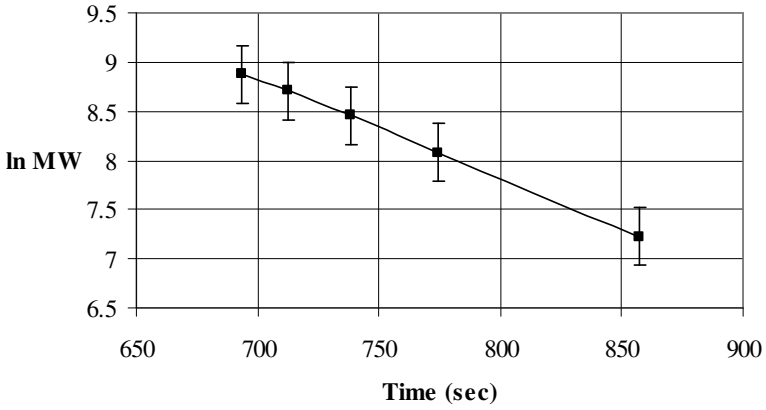

y = -98.49x + 1569.75
r = 0.9998

Figure 41. GPC retention time and mass correlation for condensation products formed in the reaction of **19** with three equivalents of **22**.

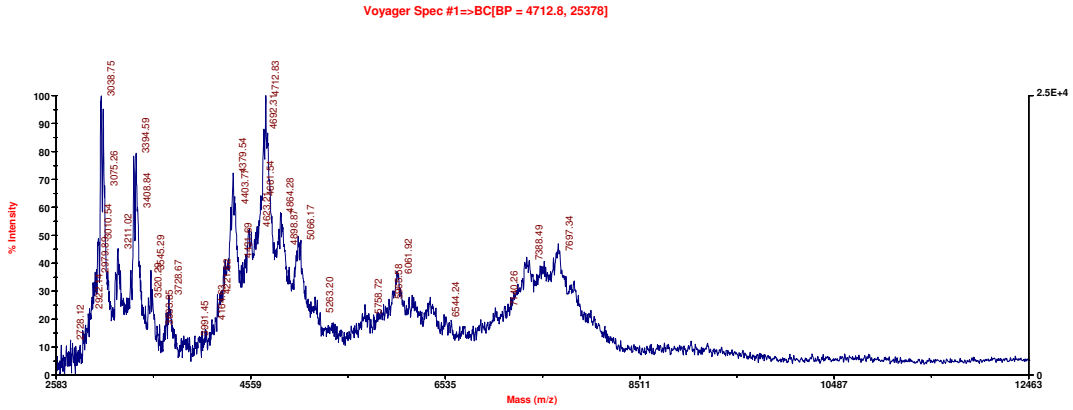

Figure 42. Partial MALDI-TOF MS of the condensation products formed in the reaction of **19** with three equivalents of **22**.

CHAPTER 4

CONCULSIONS

Lithium/bromine exchange in ethylene-cavitand **15** was successful, although complete formylation was not successful. This is most likely due to intramolecular β-elimination reaction of the ethylene spanners.

Tetrabromo propylene-cavitand **18** was successfully formylated to yield **19** by utilizing the Grignard reagent *i*-PrMgCl·LiCl. A tetrameric product was subsequently produced in the condensation of four tetratopic **19** with eight ditopic ethylenediamines. (see Figure 41)

Cavitand **19** was also shown to assemble with triamine **22**. However, a well defined structure was not produced.

CHAPTER 5

REFERENCES

1 Cram, D.J. *Science* **1983**, *219*, 1177

2 Cram, D.J.; Karbach, S.; Kim, Y. H.; Baczynskyj, G.W. *J. Am. Chem. Soc.* **1985**, *107*, 2575

3 Warmuth, R.; Yoon, J. *Accts of Chem. Research* **2001**,*4*, 95

4 Helgeson, R.C.; Paek, K.; Knobler, C.B.; Maverick, E.F.; Cram, D.J. *J. Am. Chem. Soc.* **1996**, *118*, 5590

5 Cram, D.J.; Tanner, M.E.; Thomas, R. *Angew. Chem. Int. Ed. Engl*. **1991**, *30*, 1024

4b Fujita, M. *et al*. *Chem. Commun*. **2001**, pp 509-518

5 Scheme redrawn from: Turner, D.R.; Pastor, A.; Alajarin, M.; Steed, J.W. *Structure and Bonding* **2004**, *108*, 91-168

6 MacGillivray, L.R.; Atwood, J.L. *Nature,* **1997**, *389*, 469

7 Rowan, S.J.; Cantrill, S.J.; Cousins, G.R.L.; Sanders, J.K.M.; Stoddart, J.F. *Angew. Chem. Int. Ed.* **2002**, *41*, 898

8 Figure adapted from: Rowan, S.J.; Cantrill, S.J.; Cousins, G.R.L.; Sanders, J.K.M.; Stoddart, J.F. *Angew. Chem. Int. Ed.* **2002**, *41*, 898. Used with Publisher and Author permission.

9 Ro, S.; Rowan, S.J.; Pease, A.R., Cram, D.J.; Stoddart, J.F. *Org. Lett*. **2000**, *2*, 2411

10 Liu, Xl; Warmuth, R. *J. Am. Chem. Soc.* **2006**, *128*, 14120

11 Liu, X.; Liu, Y.; Li, G.; Warmuth, R. *Angew. Chem. Int. Ed*. **2006**, *45*, 901

12 Cram, D.J. *et al*. *J. Am. Chem. Soc*. **1988**, *110*, 2229

13 Julliard *Pure Appl. Chem*. **1977**, *49,* 887

14 Compound **17** → **18** reported in reference 12, synthetic procedure modified.

15 Krasovskiy, A.; Straub, B.F.; Knochel, P. *Angew. Chem. Int. Ed*. **2006**, *45*, 159
Krasovskiy, A.; Kochel, P. *Angew. Chem. Int. Ed.* **2004**, *43*, 3333

16 Liu, Y.; Liu, X.; Warmuth, R. *Chem. Eur. J.* **2007**, *13*, 8953

17 Often, sodium or potassium adducts are seen in MALDI-TOF;
See: Gross, J.H. *Mass Spectrometry* Springer, Berlin, 2004, Ch. 10

18 DePuy, C.H.; Beedle, E.C.; Bierbaue, V.M. *J. Am. Chem. Soc*. **1982**, *104*, 6483

19 Reprinted with permission from Helgeson, R.C.; Knobler, C.B.; Cram, D.J. *J. Am. Chem. Soc.* **1997**, *119*, 3229, Copyright 1997 American Chemical Society

20 Reprinted with Permission from Cram, D.J. *et al*. *J. Am. Chem. Soc*. **1988**, *110*, 2229, Copyright 1988 American Chemical Society

CHAPTER 6

Experimental Procedures

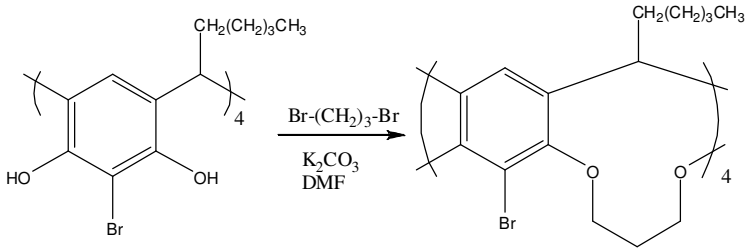

17 **18**

In-hand bromo-octol **17** (2.78 mmol, 3.015g) was dried for 4 hours under high vacuum at 120ºC along with a stirbar in a 100mL one necked flask.[14] The flask was flushed with argon, DMF (75mL) was syringed in and the solution was degassed under vacuum for 5 minutes. K_2CO_3 (3.37 mmol, 4.6g) was quickly added and 1,3-dibromopropane (11.1 mmol, 1.15 mL) was syringed into the flask. The flask is stirred for one day at 60ºC, then 1,-3-dibromopropane (11.1 mmol, 1.15mL) is added and stirring continues for 3 days at 60ºC. 1,3-dibromopropane (5.8mmol, 0.6mL) is added and the solution is stirred for 2 days at 60ºC. The reaction mixture is filtered and the solid is washed with DMF. After removal of DMF the solid is columned (SiO_2) with 20% hexanes/CH_2Cl_2 yielding white solid **18** (1.08mmol, 1.34g, 40% yield). ^{1}H NMR ($CDCl_3$) δ 0.86 (t, *j* = 7.04 hz, 12H), 1.14-1.38 (m, 24H), 1.90-2.10 (m, 12H), 2.23-2.35 (m, 4H), 3.93-4.01 (m, 8H), 4.61-4.69 (m, 8H), 4.92-4.98 (t, *j* = 7.95Hz, 4H), 7.07 (s, 4H);

^{13}C (100MHz, $CDCl_3$) 14.28, 22.73, 27.48, 29.85, 32.14, 35.42, 35.74, 70.96, 112.25, 123.76, 134.92, 154.11

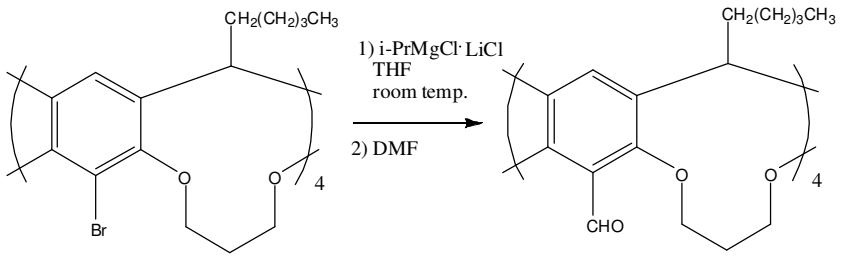

18 **19**

Tetrabromo cavitand **18** (0.066 mmol, 82 mg) is dried overnight at 120ºC in a 5mL one neck flask with stir bar. The flask is cooled to room temperature, stopped with a rubber septa, and flushed with argon. Dry THF (3 mL) is syringed in followed by i-PrMgCl·LiCl (0.5mL, 2.5 M in THF) and the solution is stirred for 3 hours at room temperature. Dry DMF is syringed in and the solution stirs at room temperature for an additional 3 hours. A suspension of off white solid forms during this time. 1M NH_4Cl(aq) (2ml) is added to the suspension and stirred for 10 minutes. The suspended material dissolves and a faint odor of amine is noted. The reaction mixture is extracted with EtOAc three times (10/5/5 mL) and the combined organics are consecutively washed with sat. $NaHCO_3$ (aq) (25mL) and brine (25mL). The organic layer is dried with $MgSO_4$ and solvent removed under reduced pressure. Purification by column chromatography is achieved by using SiO_2 stationary phase and 7.5% EtOAc/CH_2Cl_2. After column chromatography, white solid 1**9** (0.030 mmol, 31mg, 45% yield) was recovered and dried under high vacuum at 120ºC. ^{1}H NMR (400MHz, $CDCl_3$) δ 0.86 (t, *j* = 6.8 Hz, 12H, C*H*$_3$-CH$_2$-), 1.28 (m, 24H, CH$_3$-(C*H*$_2$)$_3$-CH$_2$-), 1.96 (m, 12H, -CH-C*H*$_2$-CH$_2$-, inner –O-CH$_2$-C*H*$_2$-CH$_2$-O), 2.3 (m, 4H, outer

–O-CH_2-C*H*$_2$-CH_2-O-), 3.95 (m, 8H, inner –O-C*H*$_2$-CH_2-C*H*$_2$-O-), 4.65 (m, 8H, outer –O-C*H*$_2$-CH_2-C*H*$_2$-O-), 5.0 (t, *j* = 7.7Hz, 4H, -C*H*-CH_2-), 7.4 (s, 4H, aryl-*H*), 10.3 (s, 4H, -C*H*O); ^{13}C (100MHz, $CDCl_3$) 14.28, 22.76, 30.10, 32.11, 33.41, 35.12, 73.96, 122.61, 130.68, 134.32, 158.46, 189.64; MS (MALDI-TOF) (0.5% in 1%THAP/CH_3CN) m/z = 1042.6 $[M+H]^+$,1064.6 $[M+Na]^+$, 1080.6 $[M+K]^+$; calc for $C_{64}H_{80}O_{12}$+H^+: 1042.3; Elemental Analysis: Calc. for $C_{64}H_{80}O_{12}$; C, 73.82; H 7.74. Found; C, 73.32; H, 7.79.

Further purification can be achieved with HPLC. A Varian Dynamax Microsorb 100-5 Si preparatory column (250x21.4 mm) was utilized with a sample loading of 10mg/mL, flow rate of 15mL/min, run time of 20 minutes, and solvent composition of 4% THF/CH_2Cl_2. Tetraformyl cavitand **19** eluted around 11.8 minutes.

Gel Permeation Chromatography was performed on a Varian Rainin Dual Pump HPLC equipped with dual wavelength UV/VIS detector, Eppendorf CH-30 column heater, and a Jordi GPC column (cross linked DVB; 10^3Å pore size; molecular weight cutoff ~25,000; 7.8 mm x 30 cm) with 1%TEA/CH_2Cl_2 as mobile phase at 60ºC and a flow rate of 1mL/min. The retention time for **19** is 15.9 minutes.

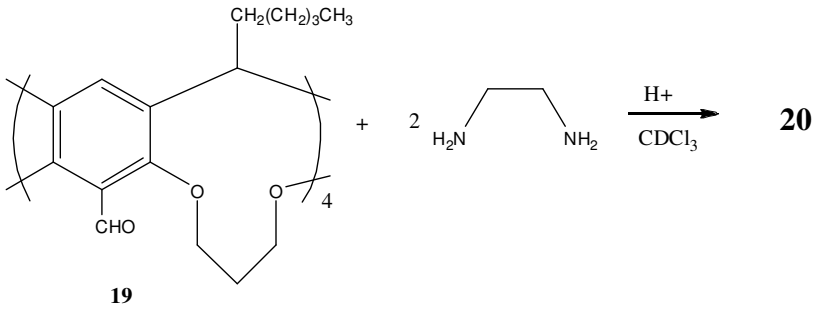

19

All chloroform is deacidified with Na_2CO_3 and dried with $MgSO_4$. Tetraformyl cavitand **19** (96μmol, 100mg) was dried under high vacuum at 120ºC in a schlenk tube. After cooling under vacuum, the tube is flushed with argon and $CHCl_3$ (10mL) is added. Ethylene-1,2-diamine (0.19mmol, 0.25m<u>M</u> in $CHCl_3$, 760 μL) is added followed by CF_3CO_2H (TFA: 0.5μmol, 1.11μL) and the solution is allowed to stand at room temperature for 15 hours under argon. A small pad of SiO_2, which was previously treated with a solution of 10% TEA/$CHCl_3$, is formed in a fritted funnel, the reaction mixture is poured through, and the pad is washed three times with $CHCl_3$ (20mL). Off-white solid **20** is obtained after rotary evaporation of solvent in 40% yield (9.6 μmol, 41.8mg). MALDI-TOF MS (0.5% in 1% THAP/CH_3CN) m/z 4359.2 $[M+H]^+$; calc for $C_{272}H_{352}N_{16}O_{32}$: m/z 4357.8

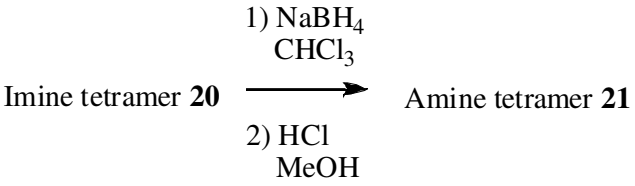

Imine tetramer **20** (57μmol, 250 mg) is dissolved in $CHCl_3$ (100mL) in a 250mL round bottom flask equipped with a stirbar and septa. $NaBH_4$ (1mmol, 37mg) is quickly added and rapid stirring is commenced under argon. Methanol (5mL) is added after 10 minutes and the reaction is allowed to vigorously stir for 72 hours at room temperature. The solvent is next removed by rotary evaporation and the remaining white solid is taken up in water (100mL) and sonicated 30 minutes producing a suspension of intermediate boramine which is filtered off. The intermediate is placed into a 250mL flask along with MeOH (150mL) and a stirbar. Stirring of the suspenstion is commenced and HCl (12.1M, approx 5mL) is titrated in until the solid dissolves. After 5 days of reflux at 70ºC, the cooled solvent is rotovaped off, yielding **21**·16HCl. Sonication for 30 minutes of **21**·16HCl in 1N NaOH(aq) and subsequent filtration yields **21** (51μmol, 225 mg, 90% yield). MS (MALDI-TOF) m/z 4392 $[M+H]^+$; calc for $C_{272}H_{384}N_{16}O_{32}$: m/z 4390.

Appendix 1. Spectrum

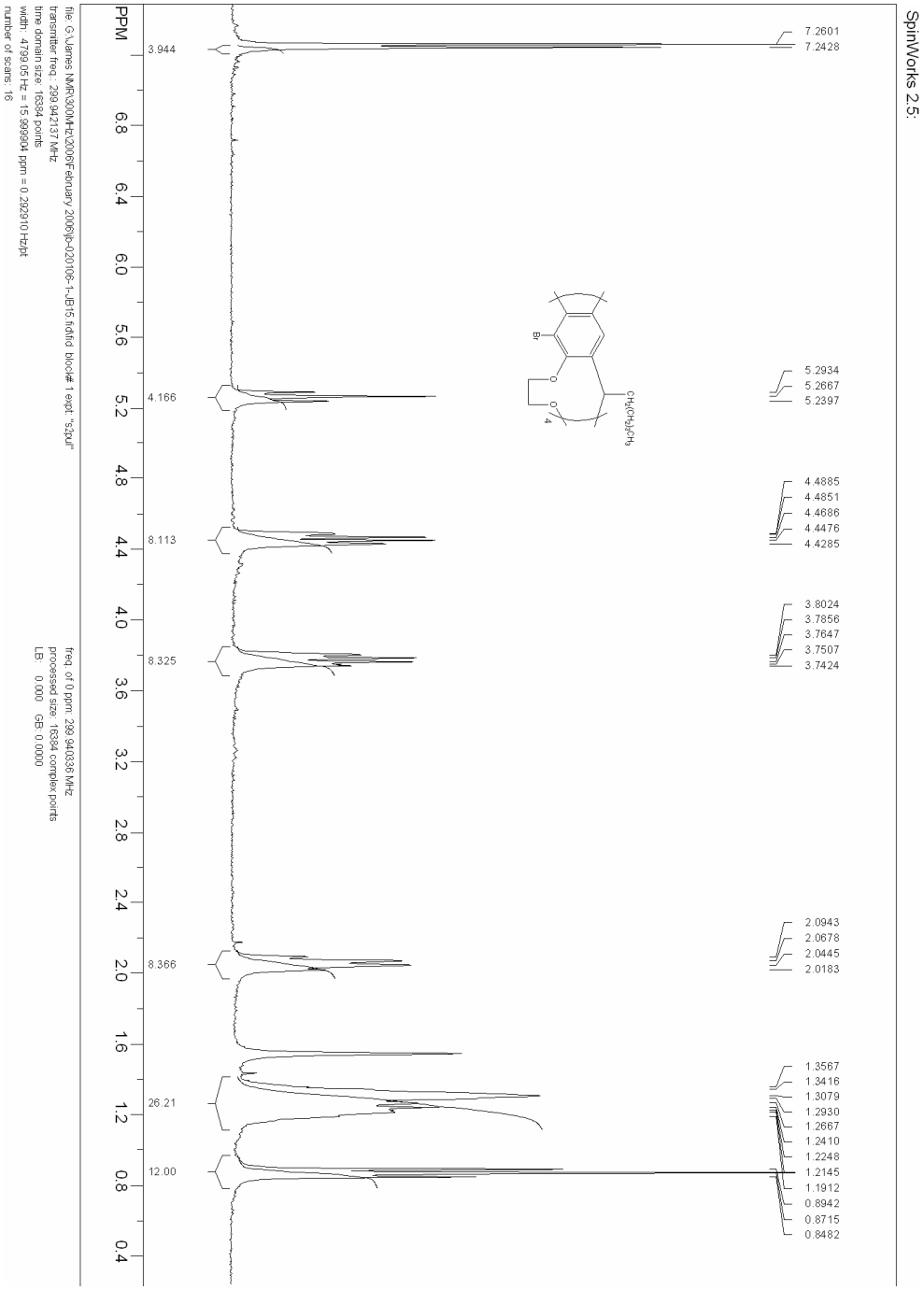

Figure 43. Tetrabromo cavitand with ethylene spanners. H_2O at δ 1.5ppm. (^{1}H NMR, 400MHZ, $CDCl_3$, 296K) See Figure 14.

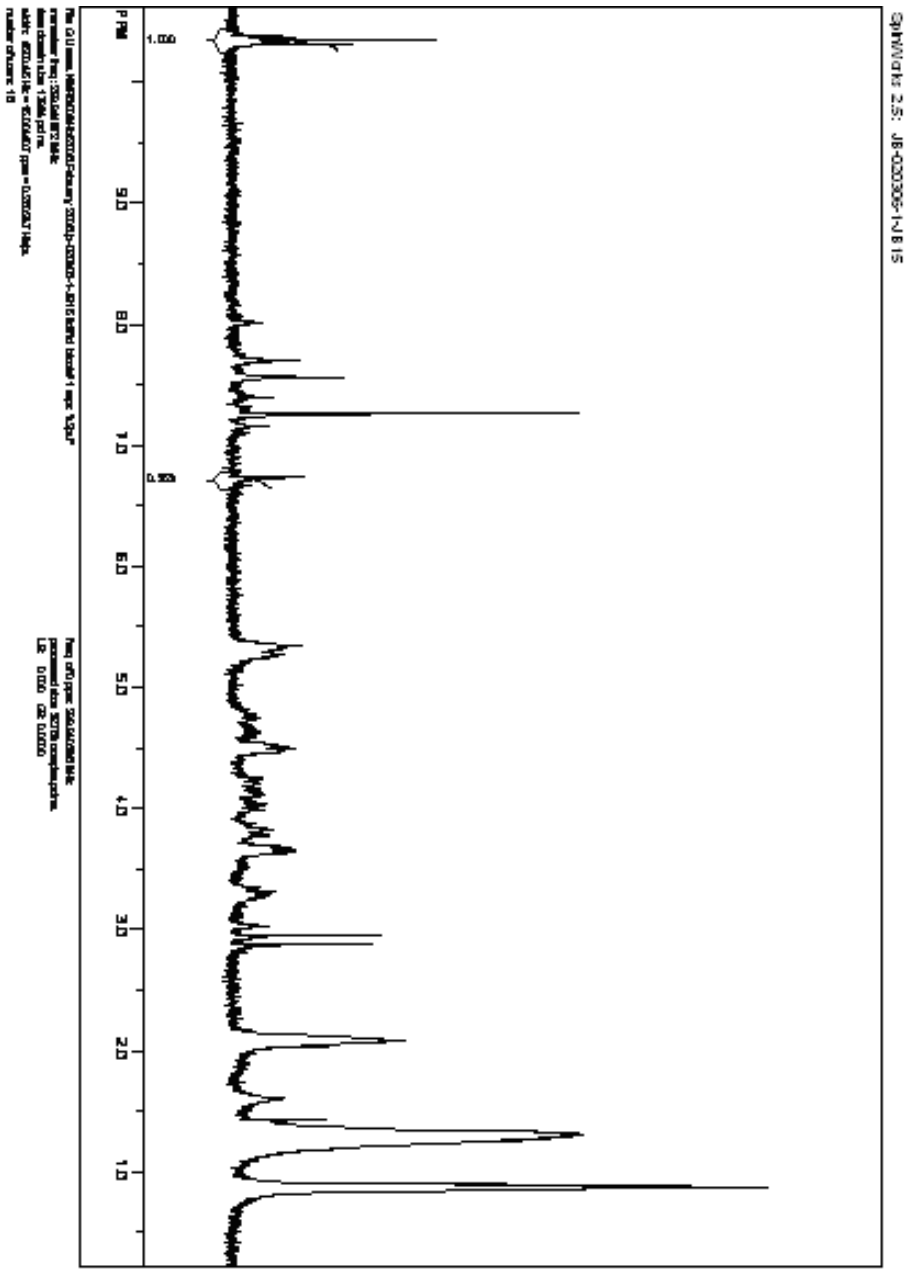

Figure 44. Full spectrum (^{1}H NMR, 400MHz, $CDCl_3$, 296K) See Figure 14

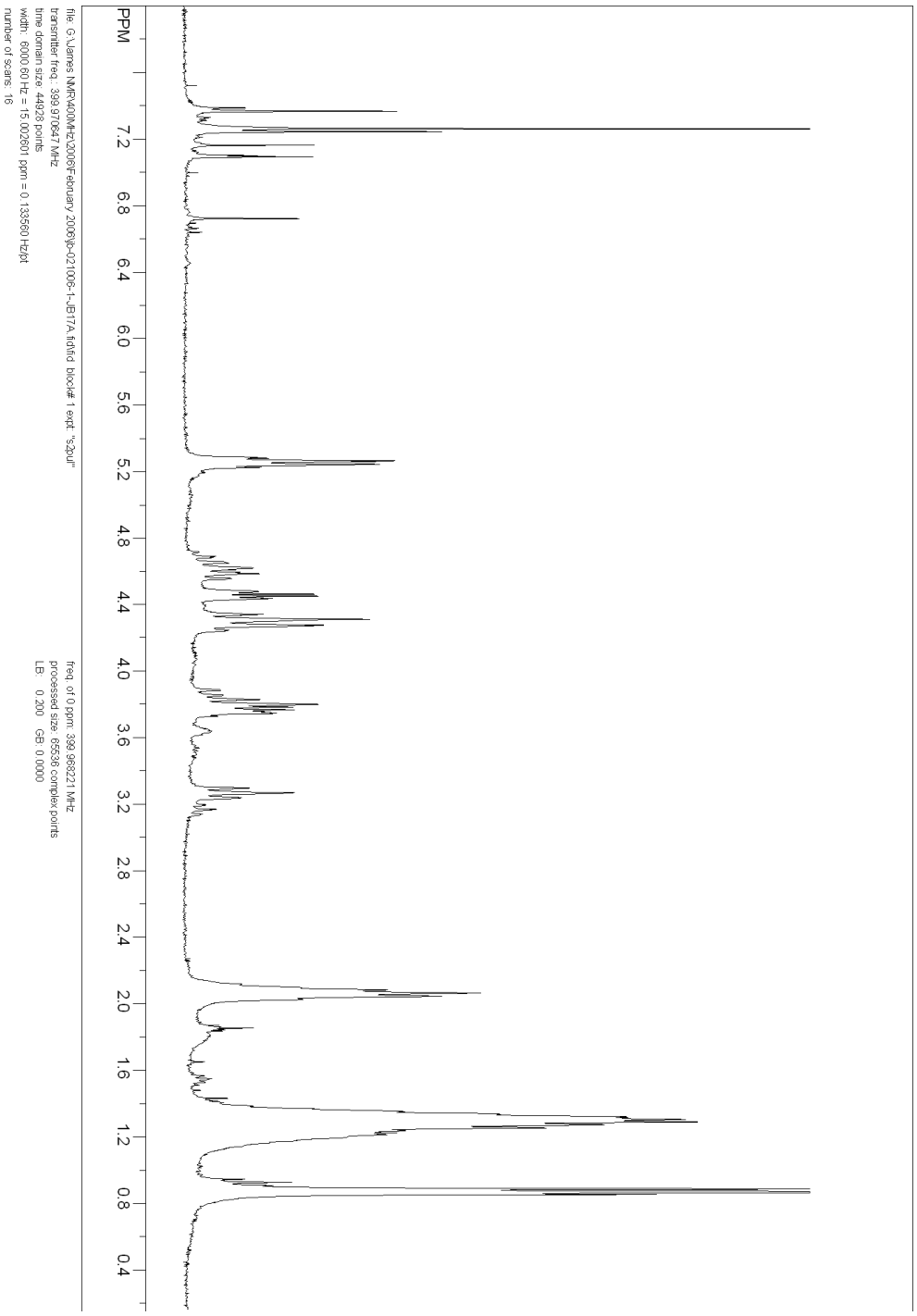

Figure 45. Full spectrum, Crude material (^{1}H NMR, 400MHz, $CDCl_3$, 296K)

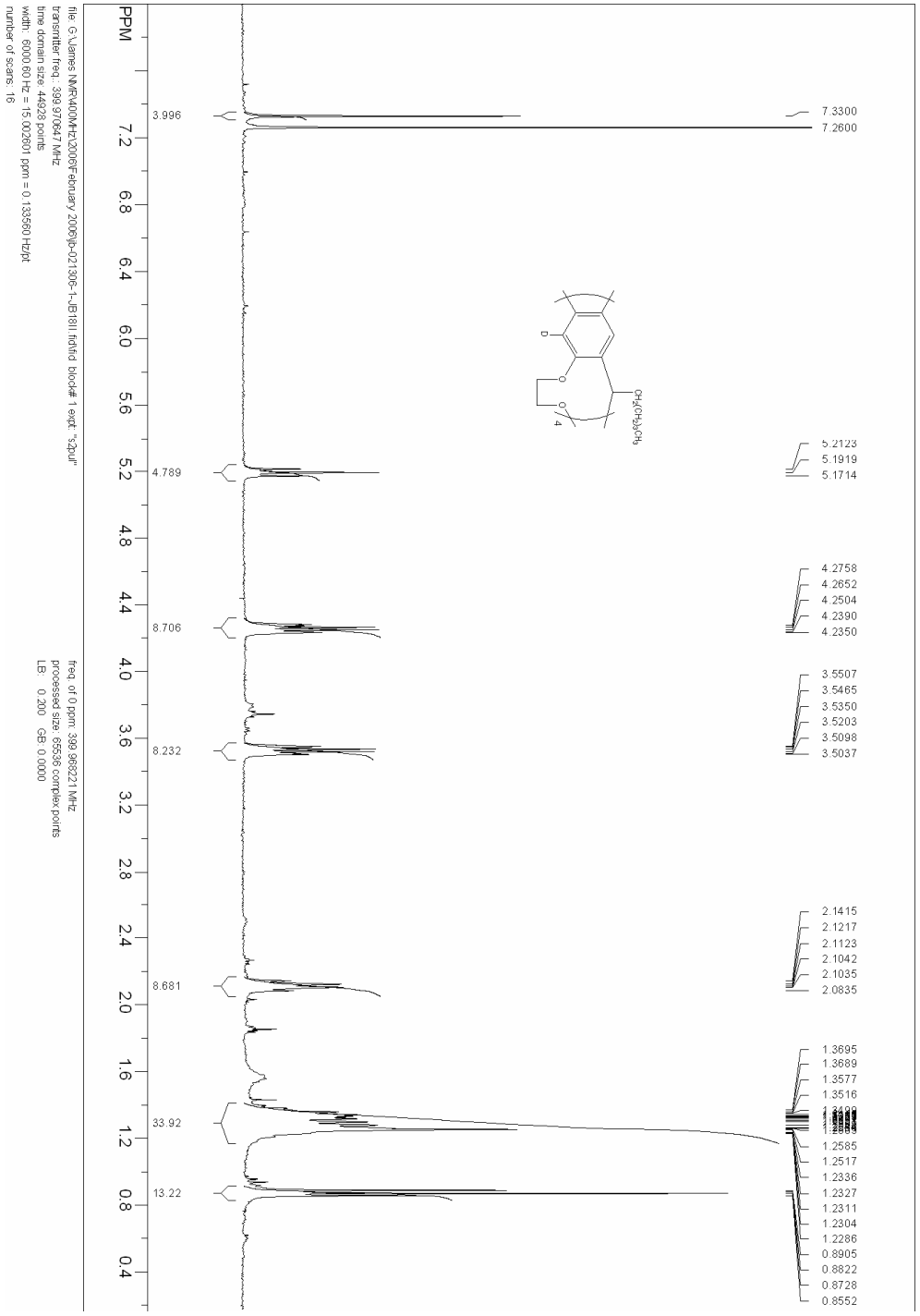

Figure 46. Full spectrum, Crude material (^{1}H NMR, 400MHz, $CDCl_3$, 296K)

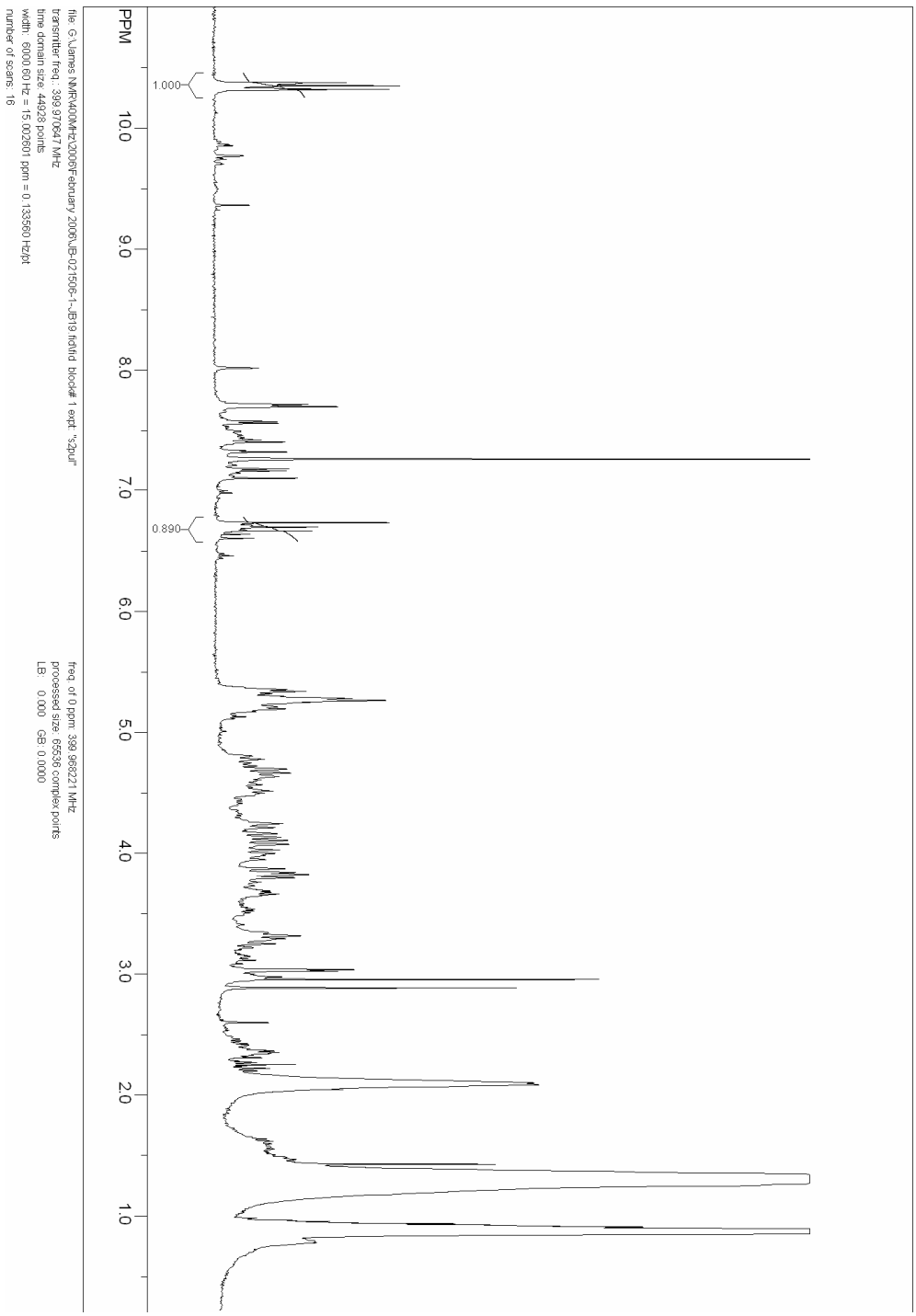

Figure 47. Full Spectrum. Crude. DMF impurity (^{1}H NMR, 400MHz, $CDCl_3$, 296K)

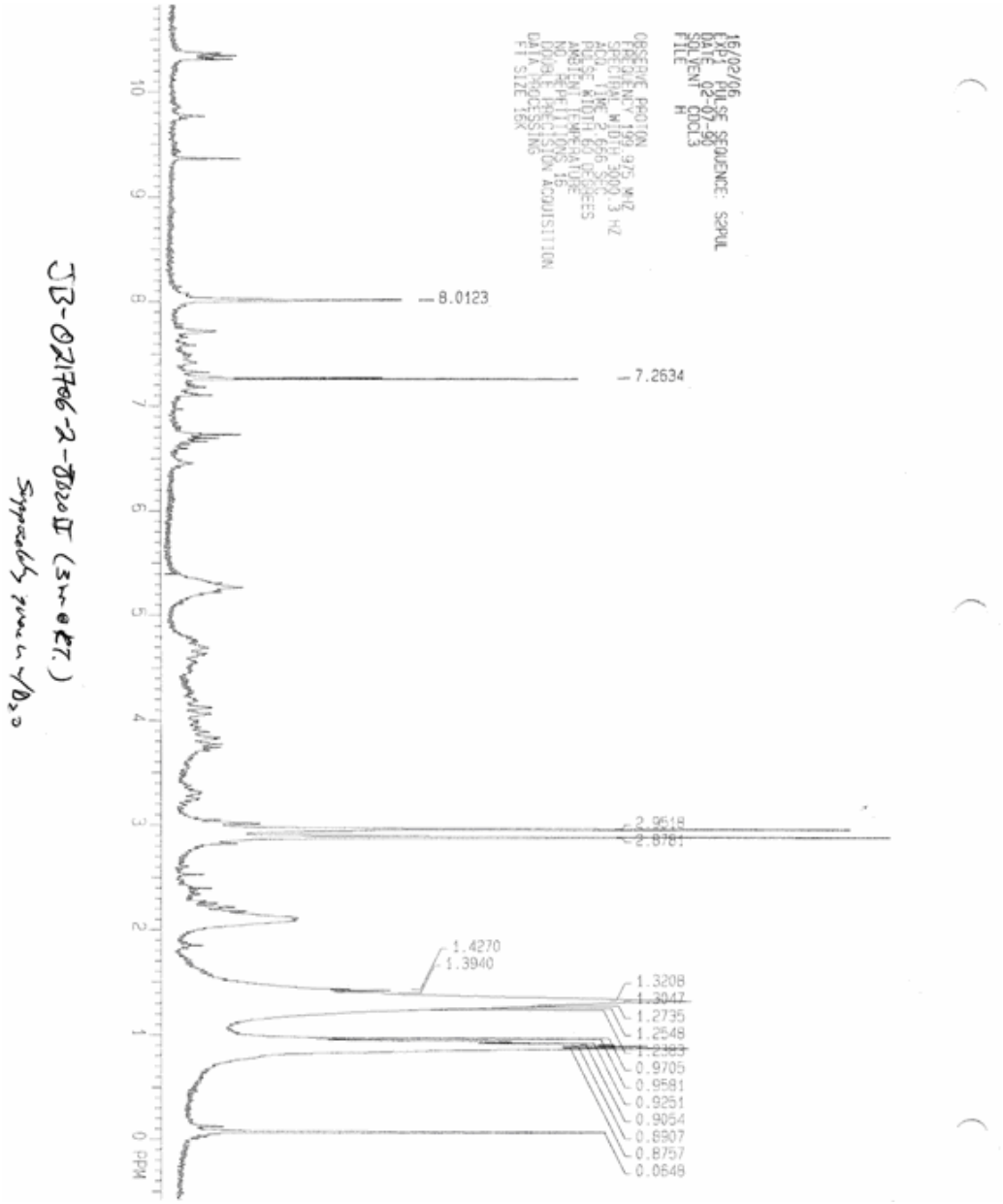

Figure 48. Full Spectrum. Crude, DMF impurity (^{1}H NMR, 200MHz, $CDCl_3$, 296K)

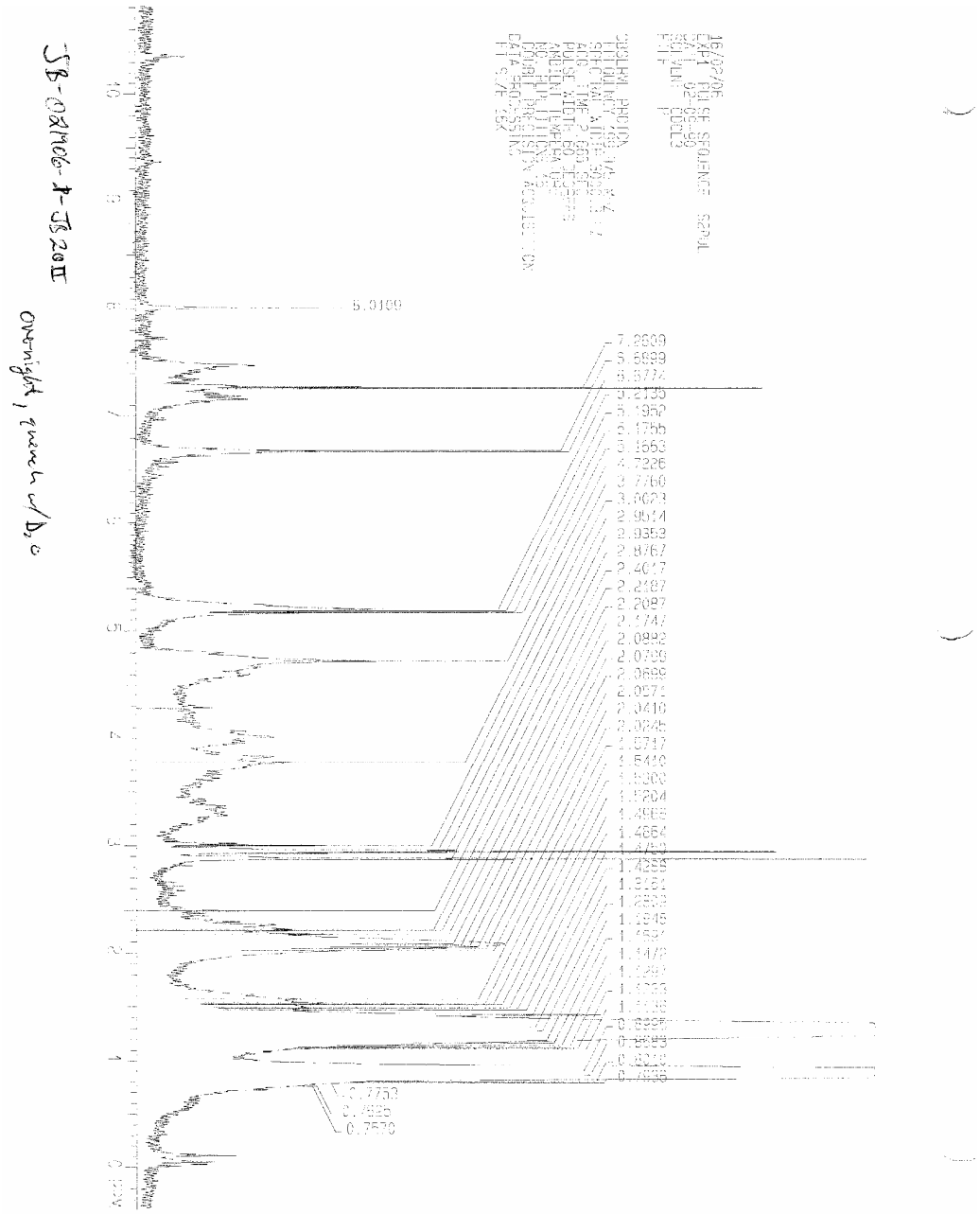

Figure 49. Full Spectrum. Crude, DMF impurity (^{1}H NMR, 200MHz, $CDCl_3$, 296K)

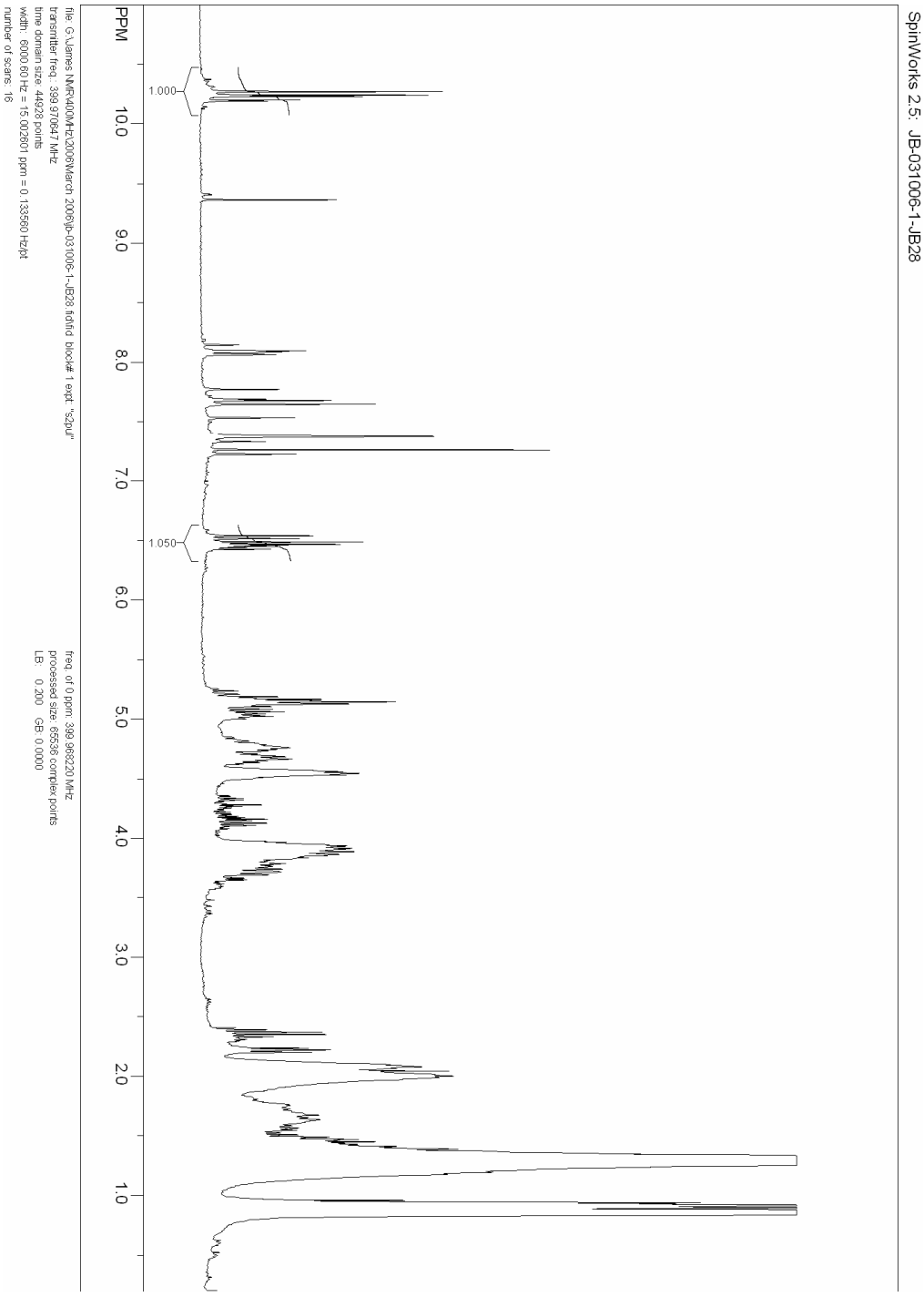

Figure 50. Full spectrum. Crude. (^{1}H NMR, 400MHz, $CDCl_3$, 296K)

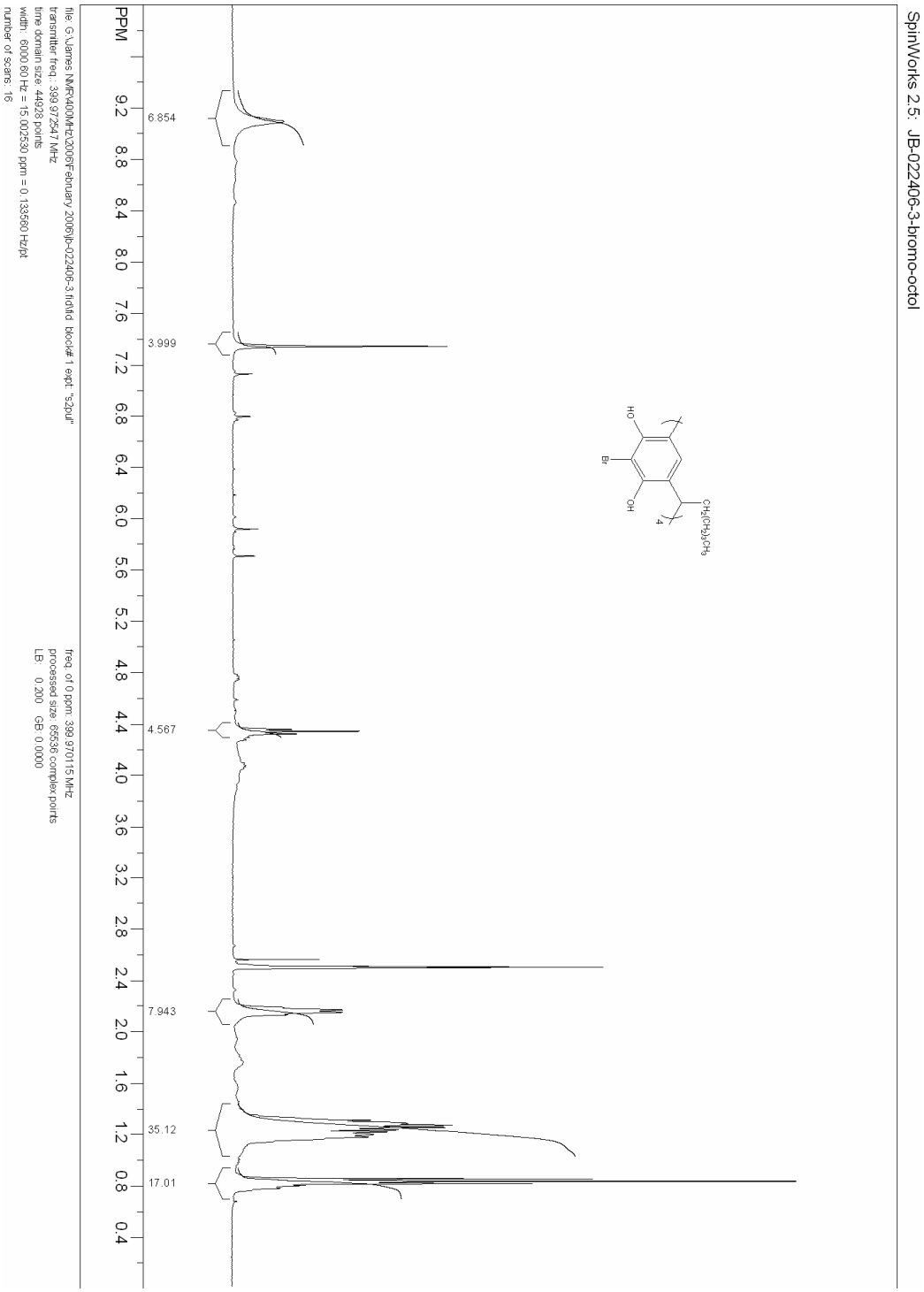

Figure 51. See Figure 24. Full Spectrum. Bromo-octol. MEK impurity. Small peaks are from known hydrogen bonded assembly. (^{1}H NMR, 400MHz, DMSO-d^6, 296K)

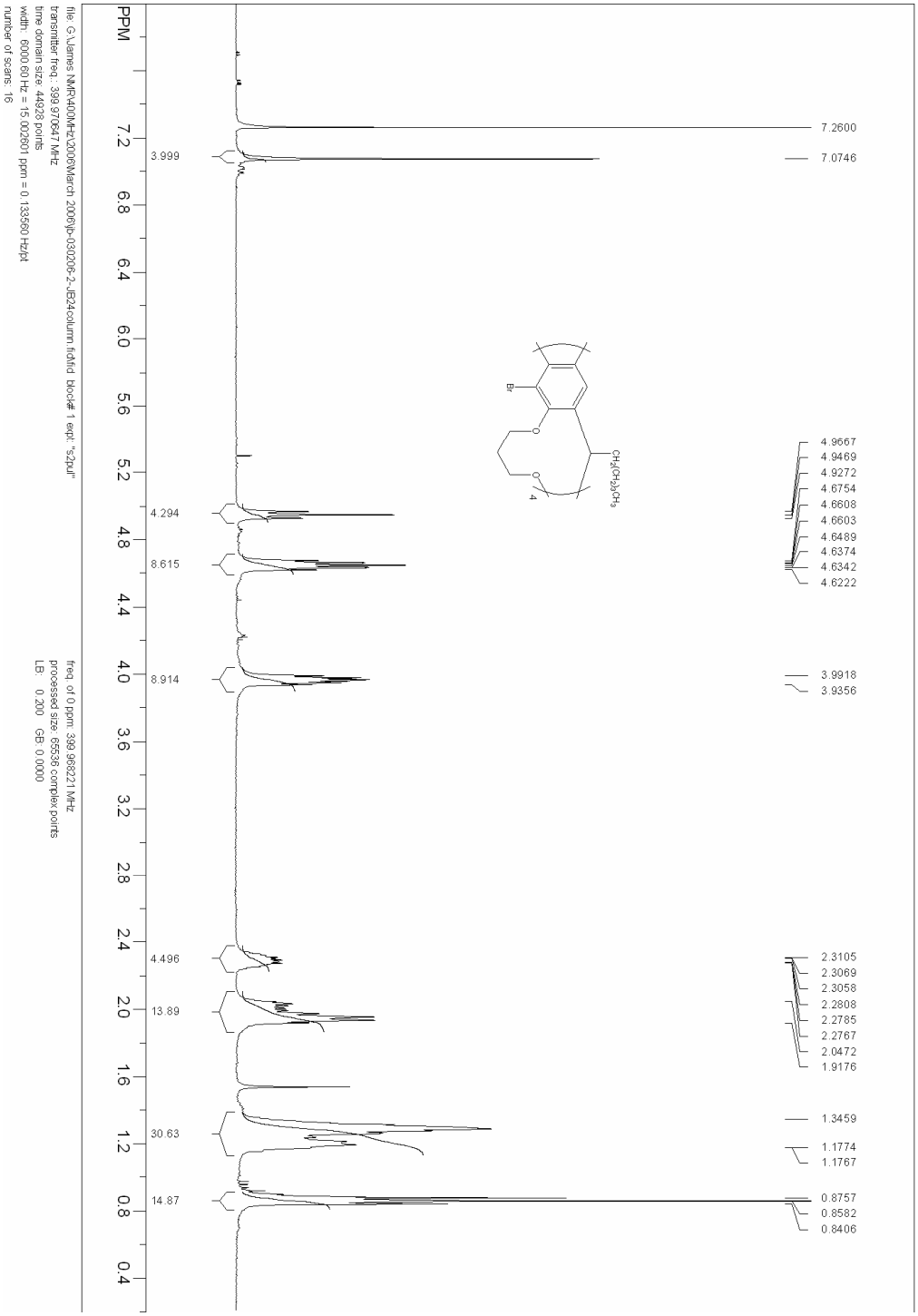

Figure 52. Compound **18**. Full spectrum. H_2O impurity. (^{1}H NMR, 400MHz, $CDCl_3$, 296K)

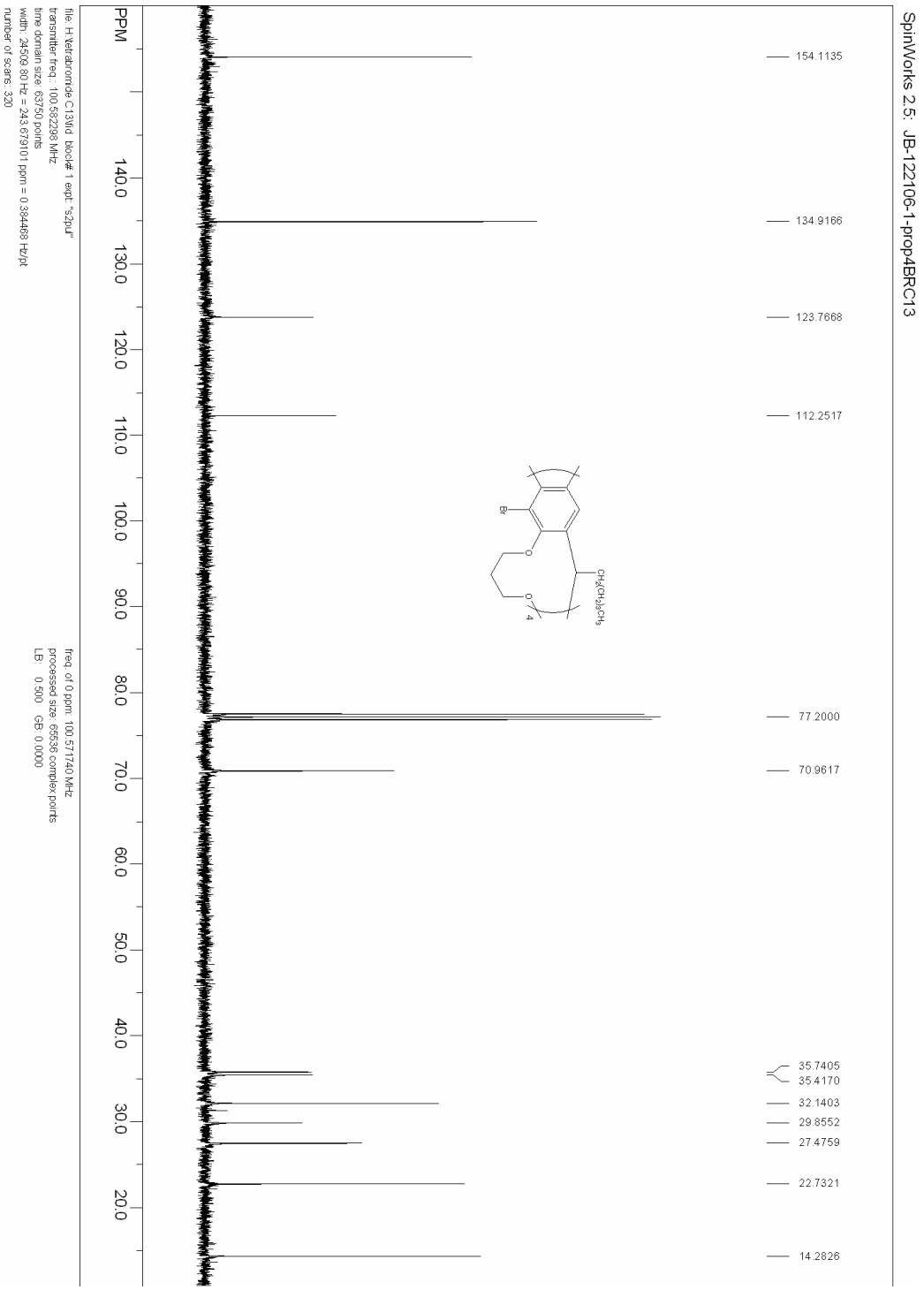

Figure 53. ^{13}C NMR of compound **18**. (^{12}C NMR, 100MHz, $CDCl_3$, 296K)

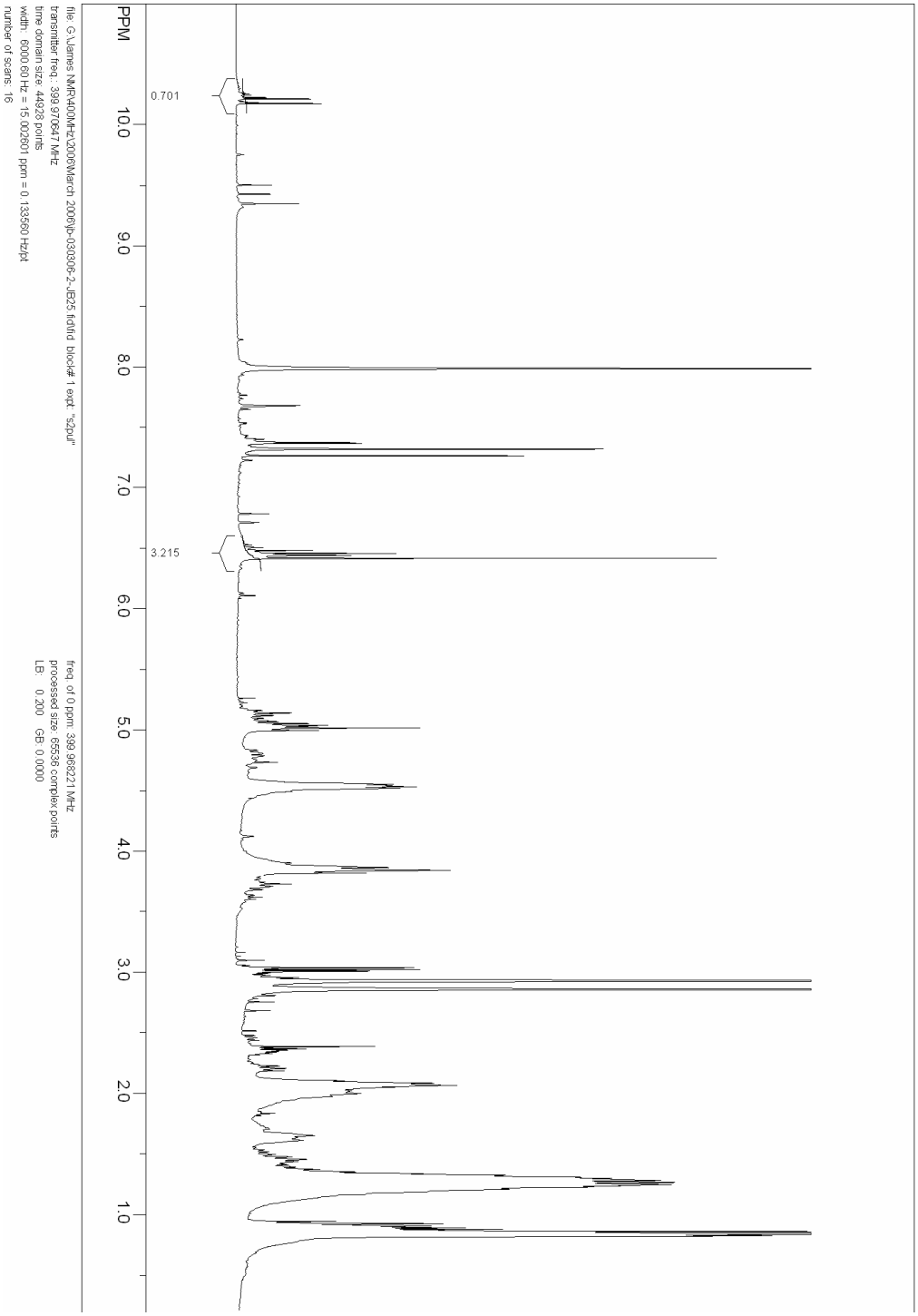

Figure 54. Crude. Full spectrum. DMF impurity. (^{1}H NMR, 400MHz, $CDCl_3$, 296K)

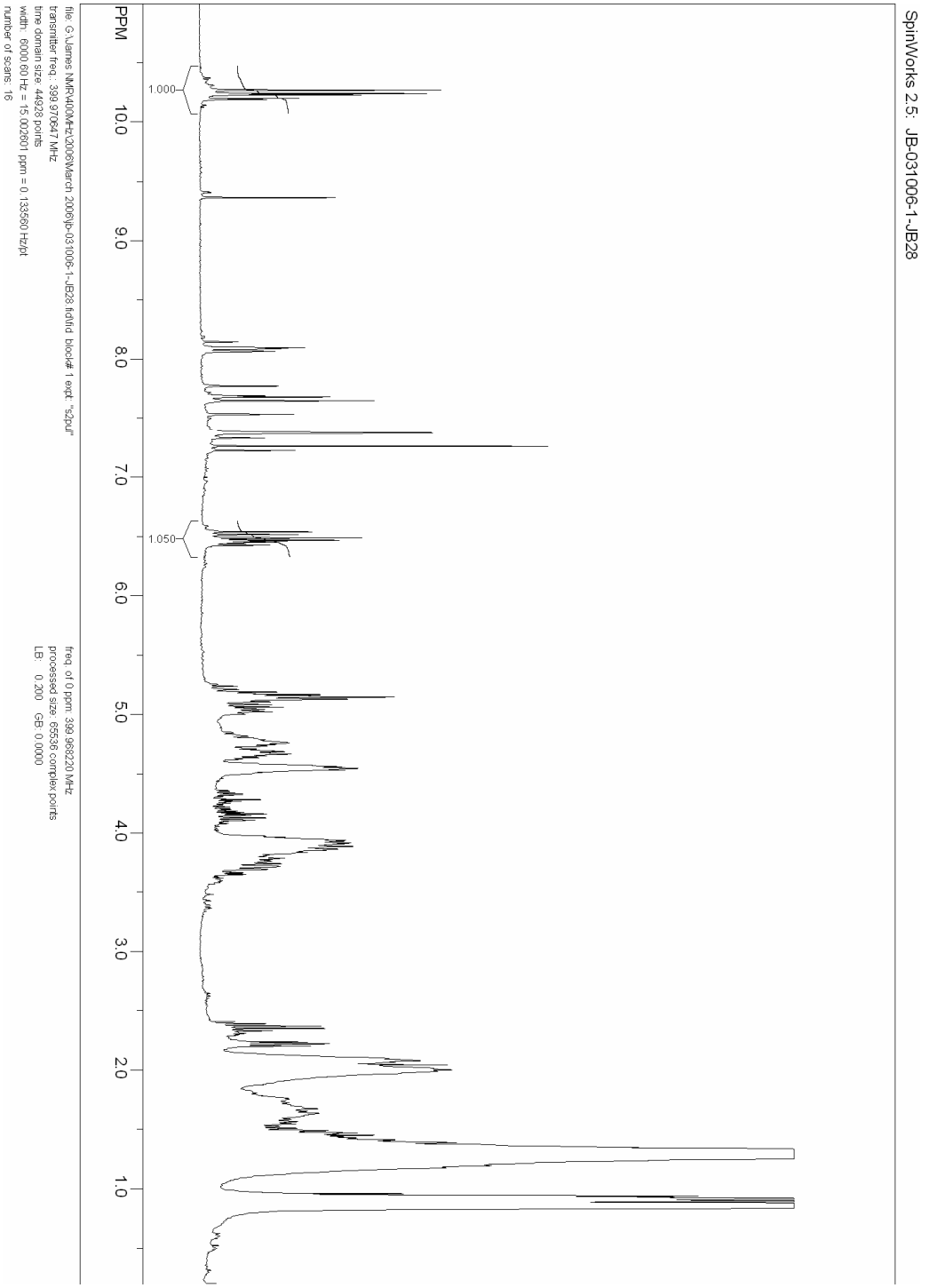

Figure 55. Full spectrum. Crude. methyl formate impurity. (^{1}H NMR, 400MHz, $CDCl_3$,296K)

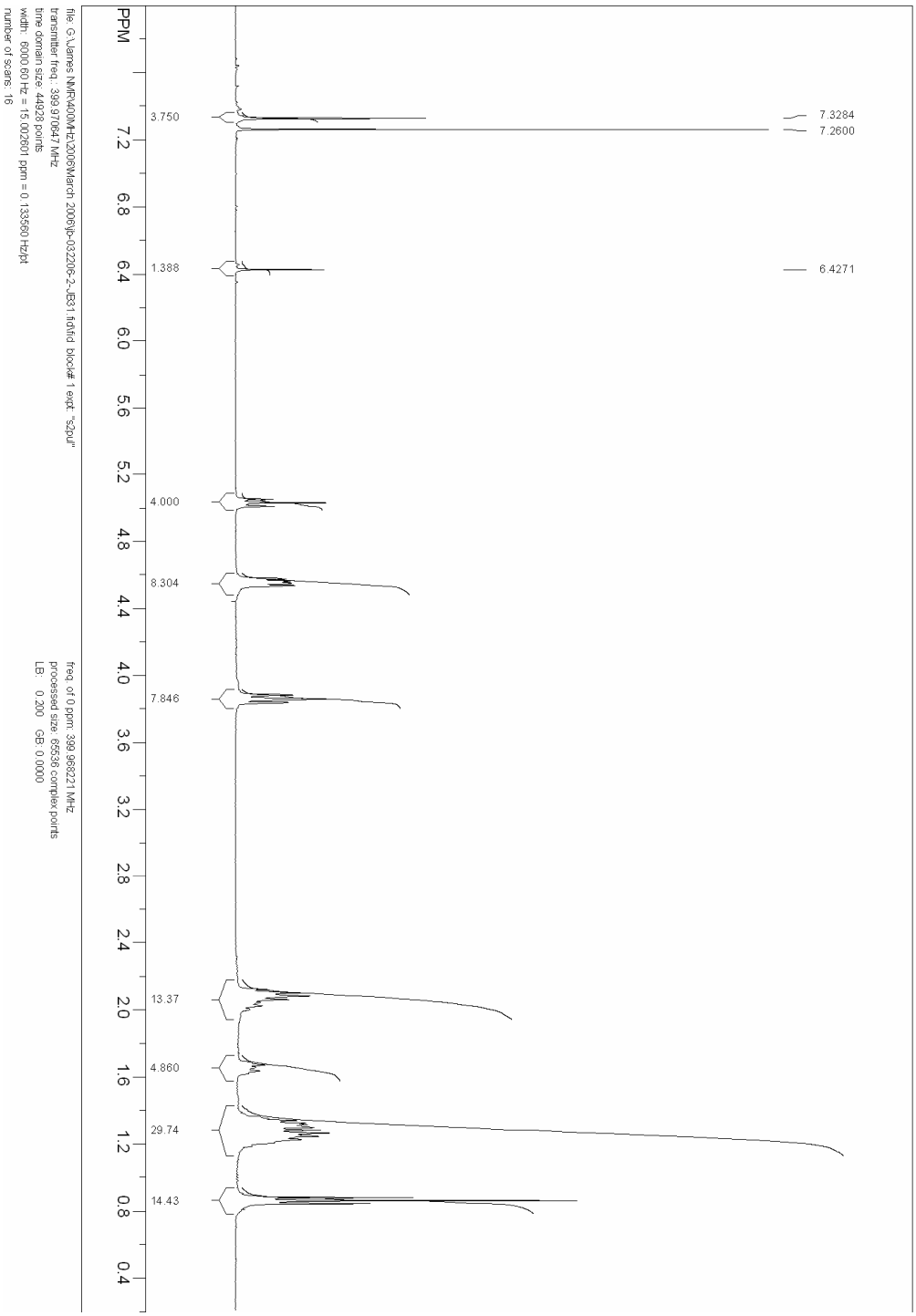

Figure 56. Full spectrum. Crude. (^{1}H NMR, 400MHz, $CDCl_3$, 296K)

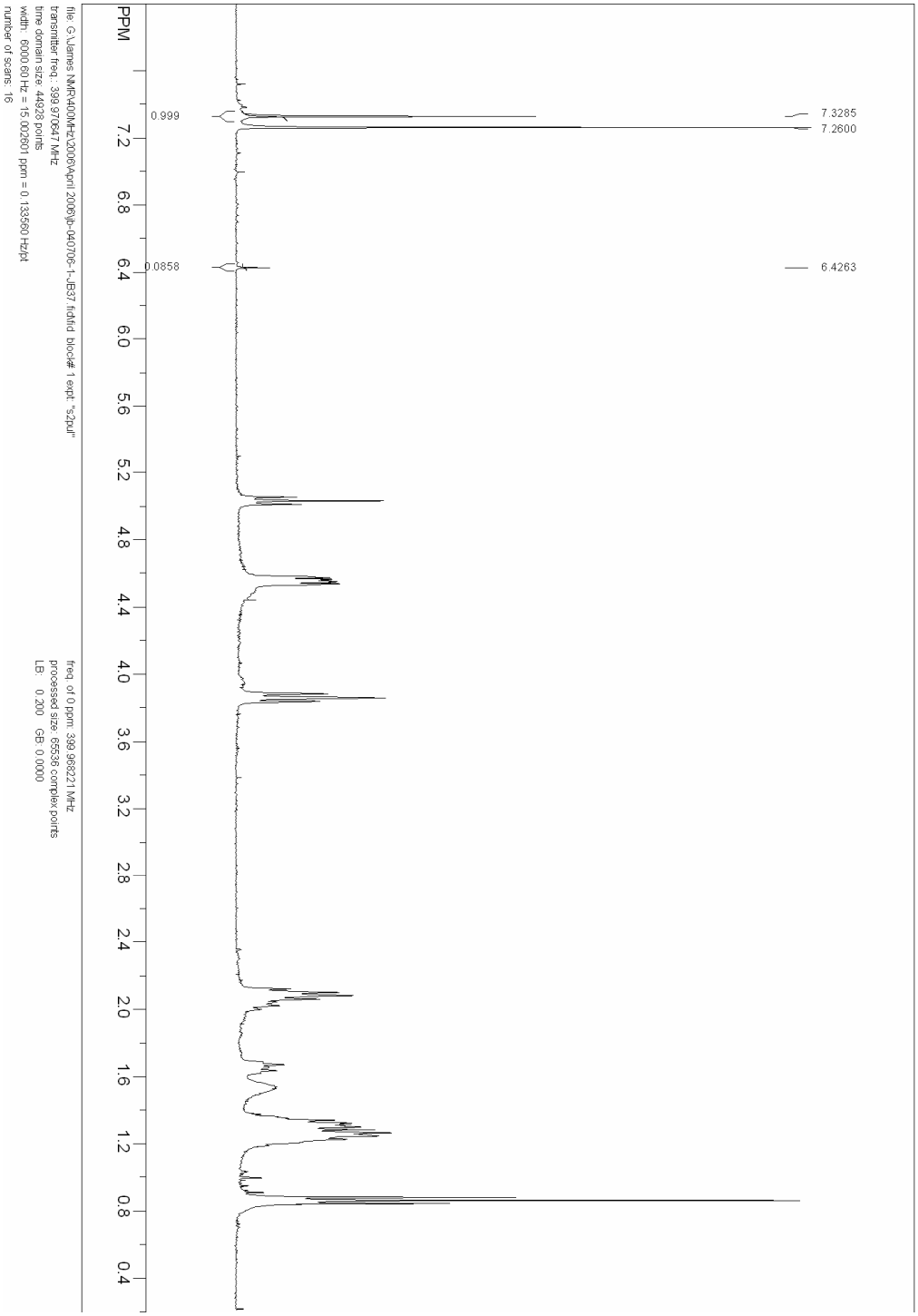

Figure 57. Full spectrum. Crude. H_2O impurity (^{1}H NMR, 400MHz, $CDCl_3$, 296K)

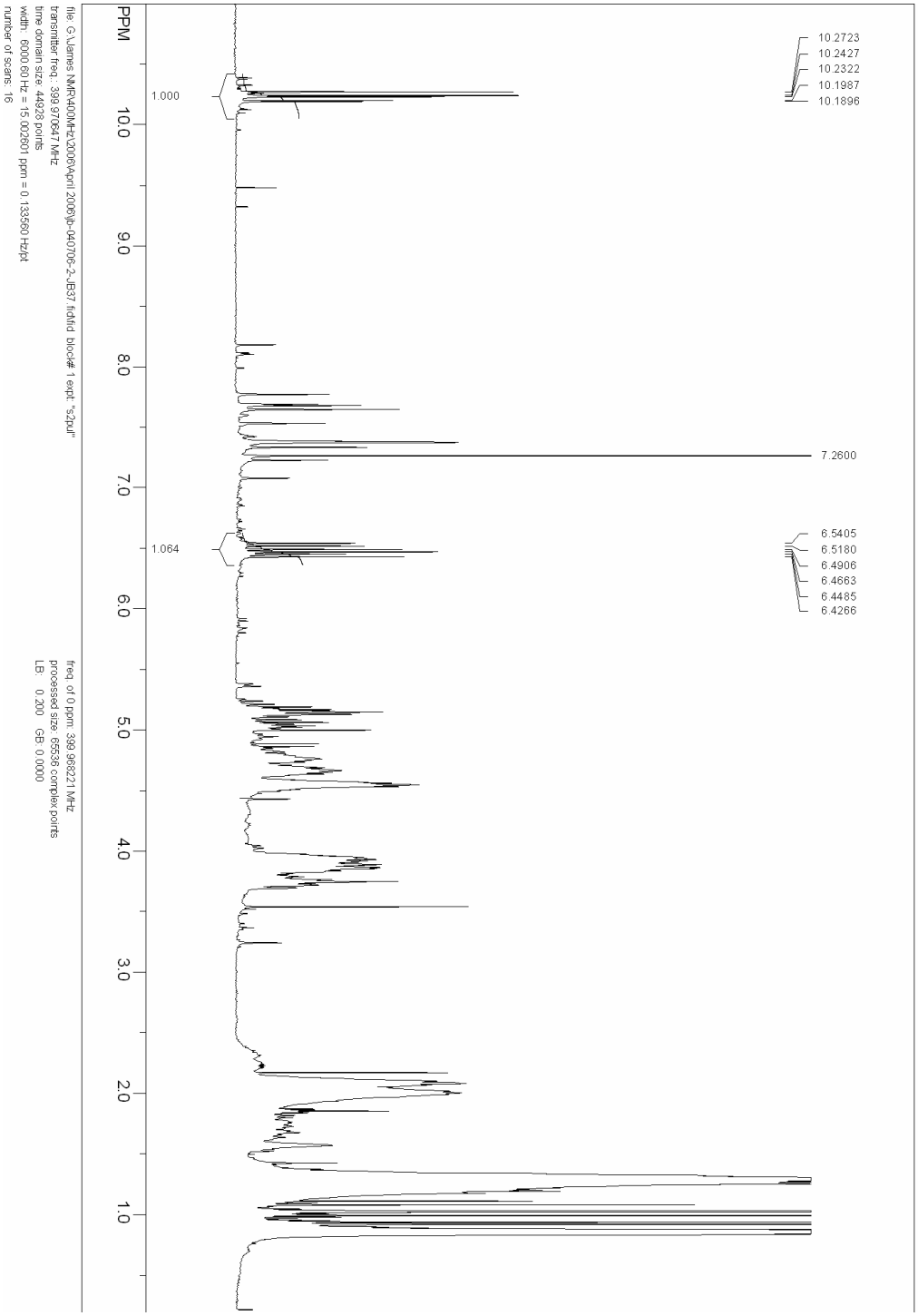

Figure 58. Formylation of **18** with methyl formate after metal-halogen exchange. (^{1}H NMR, 400MHz, $CDCl_3$, 296K)

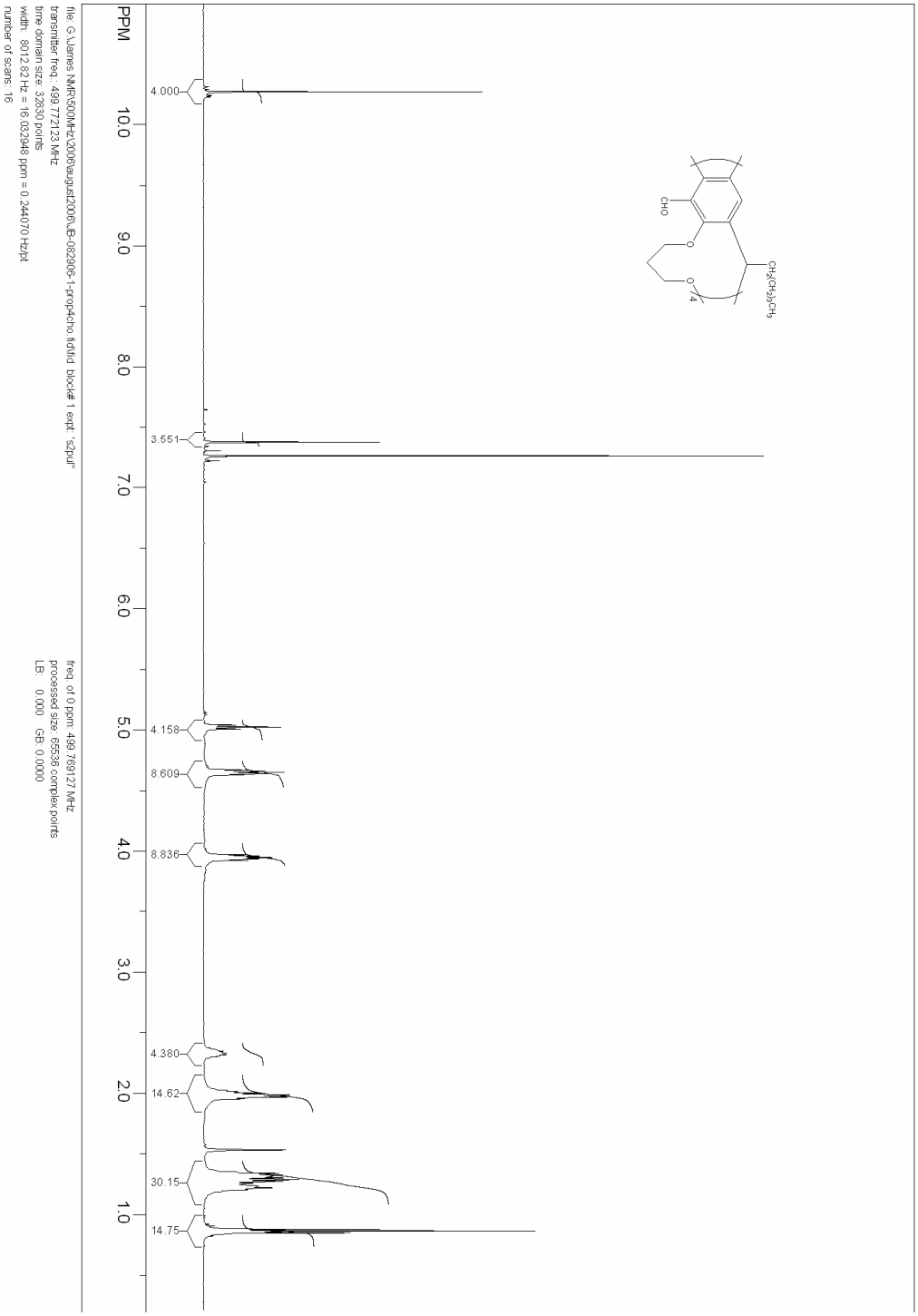

Figure 59. ^{1}H NMR for **19**. H_2O impurity at 1.5 ppm. (^{1}H NMR, 400MHz, $CDCl_3$, 296K)

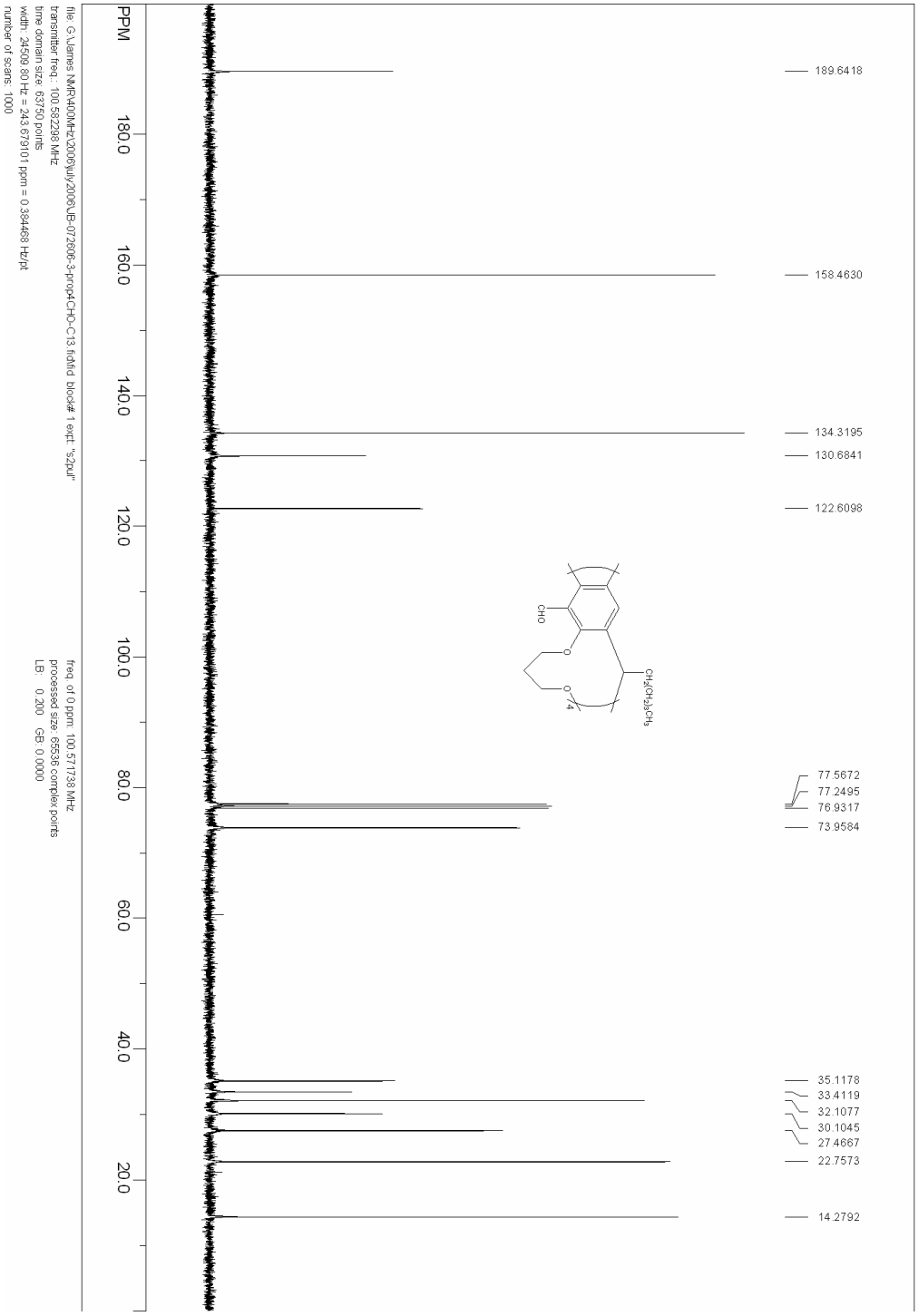

Figure 60. ^{13}C NMR of **19**. (^{13}C NMR, 100MHz, $CDCl_3$, 296K)

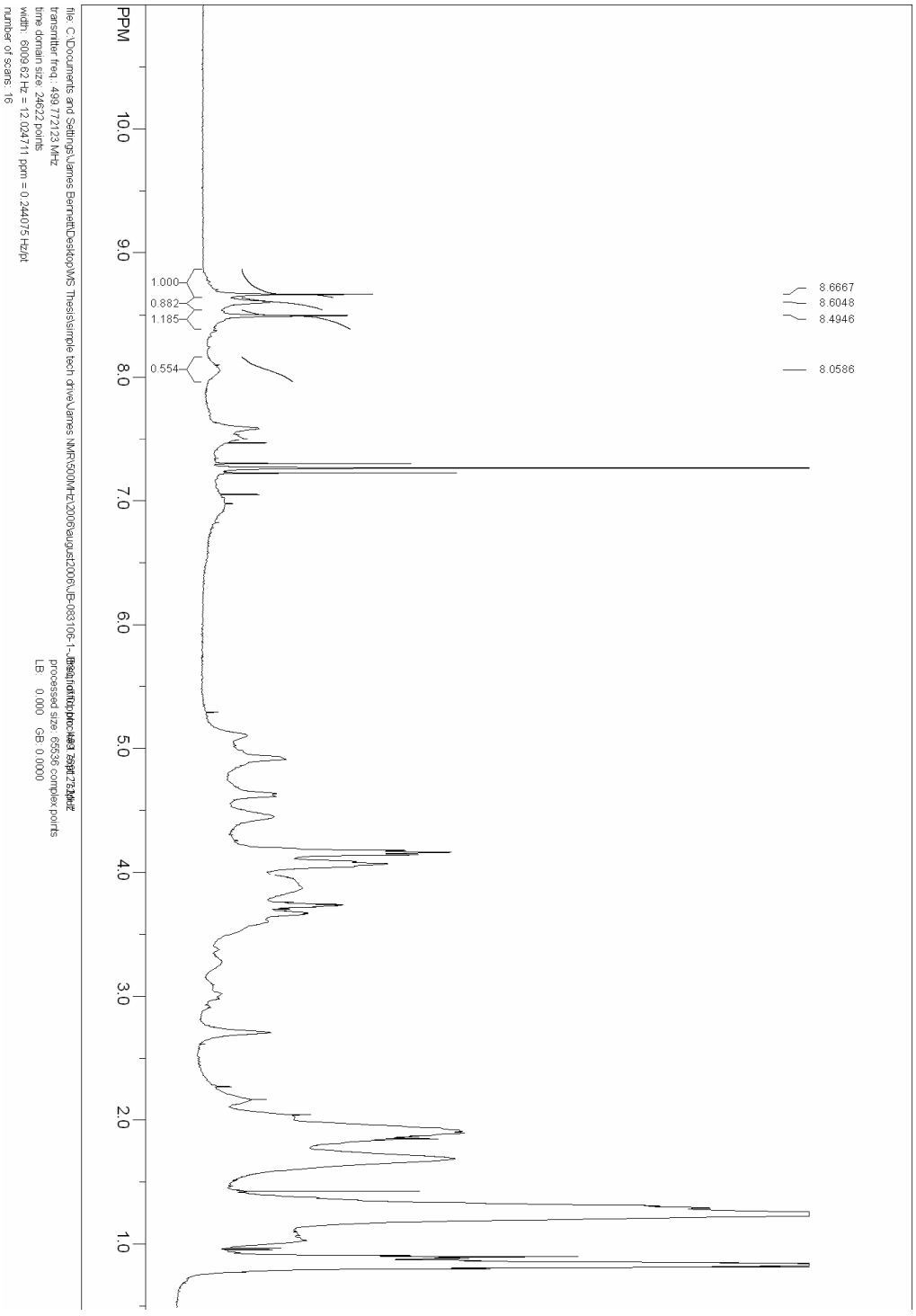

Figure 61. Tetramer **20**. Crude. (^{1}H NMR, 400MHz, $CDCl_3$, 296K)

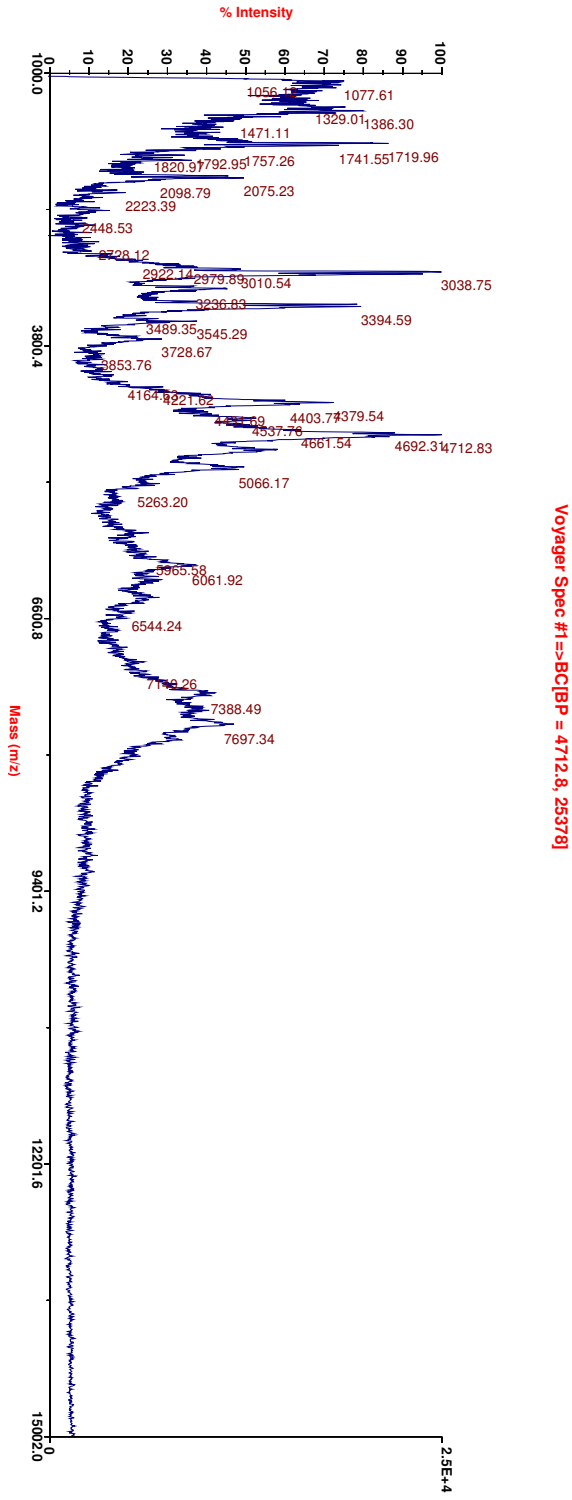

Figure 62. Tetramer Full spectrum. 0.5% in 1%THAP/CH_3CN

Appendix 2. Supporting Information

Data for figure 39. Data interpreted in Microsoft Excel

T ret	T ret (sec)	MW	ln MW
14.29	857.4	1375	7.22620901
12.91	774.6	3216.6	8.07608018
12.31	738.6	4713	8.458079927
11.87	712.2	6061	8.709630082
11.56	693.6	7170	8.877660934

Regression Statistics	
Multiple R	0.999781723
R Square	0.999563494
Adjusted R Square	0.999417992
Standard Error	1.560688036
Observations	5

	Coefficients	*Standard Error*
Intercept	1569.745227	9.851327085
X Variable 1	-98.48988127	1.188286215

Y= -98.49x + 1569.7